3-2019

Structural Transformation in Ge_xS_{100-x} ($10 \leq x \leq 40$) Network Glasses: Structural Varieties in Short-Range, Medium-Range, and Nanoscopic Scale

Y. Sakaguchi
Comprehensive Research Organization for Science and Society (CROSS)

T. Hanashima
Comprehensive Research Organization for Science and Society (CROSS)

K. Ohara
Japan Synchrotron Radiation Research

Al-Amin A. Simon
Boise State University

M. Mitkova
Boise State University

Structural transformation in Ge_xS_{100-x} ($10 \leqslant x \leqslant 40$) network glasses: Structural varieties in short-range, medium-range, and nanoscopic scale

Y. Sakaguchi,[1,*] T. Hanashima,[1] K. Ohara,[2] Al-Amin A. Simon,[3] and M. Mitkova[3]

[1]*Neutron Science and Technology Center, Comprehensive Research Organization for Science and Society (CROSS), Tokai, 319-1106, Japan*

[2]*Japan Synchrotron Radiation Research Institute, SPring-8, Sayo-gun, Hyogo 679-5198, Japan*

[3]*Department of Electrical and Computer Engineering, Boise State University, 1910 University Dr., Boise, Idaho 83725-2075, USA*

(Received 8 August 2018; revised manuscript received 14 January 2019; published 19 March 2019)

Precise x-ray diffraction measurements using high-energy x rays of synchrotron radiation and systematic Raman scattering measurements were carried out for Ge_xS_{100-x} ($10 \leqslant x \leqslant 40$) network glasses. The structural models of the network glasses were proposed based on the results. In the stoichiometric composition $Ge_{33}S_{67}$, GeS_4 tetrahedral units are connected forming either corner-sharing or edge-sharing structures. In the S-rich glasses, S atoms are inserted between two neighboring GeS_4 tetrahedra, resulting in a flexible *floppy* network. In a much more S-rich region, some S_8 ring molecules are isolated from the network, and assemble to form a crystal in nanoscopic scale. In this respect, $Ge_{10}S_{90}$ samples are regarded as crystallized glasses. In the Ge-rich region, the GeS_4 tetrahedra are connected with *bridging* Ge atoms. The connection makes a new *rigid* network. The *bridging* Ge-S bond is weaker than the intratetrahedron bond, and this leads to drastic changes in the optical properties.

DOI: 10.1103/PhysRevMaterials.3.035601

I. INTRODUCTION

There has been considerable interest in amorphous chalcogenide semiconductors for more than 40 years because of their diverse functionality, in which the physical properties change by applying a specific external field like light illumination [1–3]. Among various amorphous chalcogenides, Ge-S (Se) glassy binary alloy is one of the most studied materials because of its simplicity, in which the system is composed of only two elements, and its structural variations. The Ge-S (Se) system has a good glass-forming ability in a wide composition range [4,5]. The network structure is built up with fourfold-coordinated Ge atoms and twofold-coordinated S (Se) atoms. The nature of the network is considered to change with increasing Ge [or S (Se)] content. Phillips [6] regarded the number of constraints per atom, N_{CO}, and provided the optimum concentration for glass-forming ability in Ge_xSe_{1-x} system as $x = \frac{1}{6}$. The network is under constraint for $x < \frac{1}{6}$, while it is over constraint for $x > \frac{1}{6}$. At $x = \frac{1}{6}$, the mean coordination $\langle r \rangle$ should be $r_p = 2.33$. Thorpe [7] referred $x < \frac{1}{6}$ as "floppy" region in which the network is like a polymeric glass, while he referred $x > \frac{1}{6}$ as "rigid" in which the network is like amorphous solid. There should be a rigidity percolation transition across r_p in the system. After 17 years from their suggestions, Thorpe and Phillips and their related researchers, more specifically Boolchand, pointed out that there can also be a narrow third region around r_p, what they call "*intermediate phase*," where the network is rigid, but stress free [8–12]. Overall, these possibilities indicate varieties in the network system in Ge-S(Se) alloys.

So far, the microscopic "molecularlike" structure in glassy Ge-S(Se) system has been mainly investigated by Raman spectroscopy. At $x = 0.33$ [$GeS(Se)_2$], there are $GeS(Se)_{4/2}$ tetrahedral units which also exist in $GeS(Se)_2$ crystal. The presence of the units is confirmed by the Raman peak, assigned to the breathing mode of methanelike $GeS(Se)_{4/2}$ molecules (for corner-sharing tetrahedra) [13,14]. SiO_2 glasses have only such corner-sharing tetrahedra $SiO_{4/2}$. However, Ge-S(Se) glasses have also edge-sharing tetrahedra. Furthermore, Ge-S(Se) glasses can have homopolar Ge-Ge and S-S (Se-Se) bonds, whereas SiO_2 glasses have only Si-O heteropolar bonds. In the Raman spectra, the Ge-Ge bonds can be found from the vibrational mode of $S(Se)_3$-Ge-Ge-$S(Se)_3$ ethanelike unit [15]. Moreover, we have suggested from theoretical considerations that there would be single chains, including Ge-Ge or S-S (Se-Se) homopolar bonds, in Ge-rich Ge-S glasses [16], although an experimental evidence is required for the validity.

Ge-S(Se) alloys have also received considerable attention due to the possibility for silver photodiffusion, which is a specific photoinduced effect in chalcogenide films. It was reported in 1966 [17] and has been used in diverse applications such as photoresist [18], the fabrication of relief images in optical elements [19], and nonvolatile memory devices [20,21]. It is interesting to know how silver ions diffuse in the chalcogenide layer, and there have been considerable works on the kinetics [22]. Recently, the authors performed neutron reflectivity measurement of Ag/Ge-chalcogenide films and found that the kinetics of the silver photodiffusion markedly depends on the Ge composition [23–27]. Such Ge composition dependence is attributed to the difference in the structure of amorphous Ge-S alloy. Therefore, it is important to clarify the structure of amorphous Ge-S alloy for various Ge compositions.

*y_sakaguchi@cross.or.jp

The diffraction study can provide important information on the local and the medium-range structure, and could be a useful technique to explain the Ge composition dependence on Ag photodiffusion in Ge containing glasses. Systematic x-ray diffraction measurements were performed by Fueki *et al.* for 10 x 40 [28]. However, the measured Q range was limited up to 13.5 $Å^{-1}$ because of the used x-ray source, which was generated by Mo target. Detailed discussion on the pair distribution functions would be difficult due to the limitation of the Q range. In recent years, excellent works have been done on the structure of Ge-S binary glasses using synchrotron radiations and neutron sources for the S-rich glasses by Bychkov *et al.* [29] and for the Ge-rich glasses by Bytchkov *et al.* [30]. However, the analysis has not been done in a unified way through the whole glass-forming range, including both S-rich and Ge-rich regions.

In this paper, we performed precise measurements of x-ray diffraction of Ge-S binary glasses for wide Ge-composition region, 10 x 40, using the synchrotron radiation at SPring-8 and compare the result with systematically measured Raman spectra. Based on the results, we discuss the structural variations in the glasses in terms of the short-range, medium-range, and nanoscopic orders, and explain the composition dependence of the physical properties of Ge-S glasses.

II. EXPERIMENT

Ge_xS_{100-x} ($x = 10, 20, 30, 33, 40$) glasses were prepared by quenching the melts with exactly measured quantities of Ge and S with purity 99.999, placed in fused silica ampoules evacuated to 10^{-5} Torr. In order to obtain homogeneous glasses the synthesis of each composition was carried out for 7 days and the quenching was performed at a temperature 50 °C above the glass transition temperature of the particular mixture. The composition of the glassy material was checked applying Energy Dispersive Spectroscopy (EDS) using a Hitachi S-3400N EDS system. The results were acquired by averaging data over five points on each sample. The analysis revealed that within the resolution of the system the composition of the samples corresponds to the one planned for the five samples synthesized for the experiment.

The high-energy x-ray diffraction experiments were carried out at the bending magnet beamline BL04B2 [31] of SPring-8 with a two-axis diffractometer for disordered materials [32]. The incident photon energy of 61.7 keV, which was obtained from a bent Si (220) crystal, was used for the experiment. The measurements were performed in transmission geometry. The intensity of the incident x ray was monitored by an ionization chamber filled with Ar gas and the scattered x rays were detected by a CdTe solid-state detector. The collected data sets were corrected for the absorption, the background, and the polarization. Details of the data correction and the normalization procedures are given in [33].

The Raman spectra were measured at room temperature using a Raman spectrometer (JASCO, NRS-7500) with the laser excitations of 532 and 785 nm. The relationship between the excitation energy and the absorption edge of the glasses will be shown in Sec. III (Fig. 5).

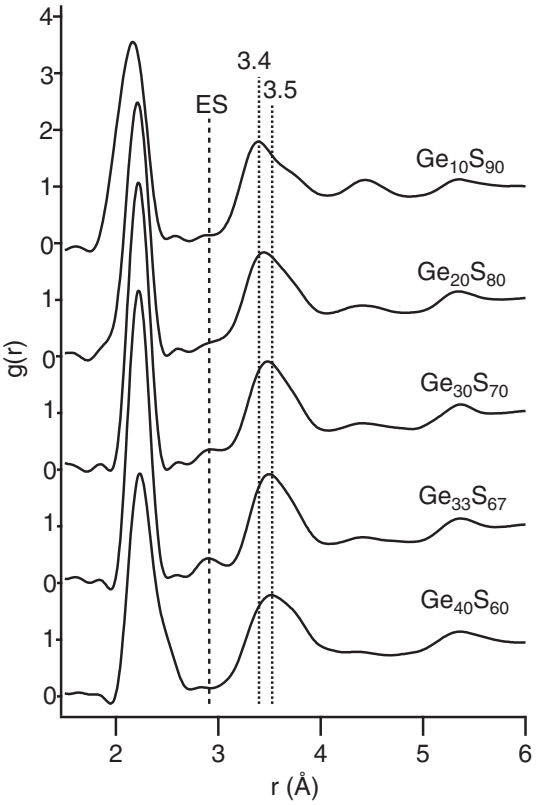

FIG. 1. Pair distribution functions of Ge_xS_{100-x} ($x = 10, 20, 30, 33, 40$) glasses. The broken line, indicated by "ES," shows the position where the peak associated with the Ge-Ge distance between two neighboring edge-sharing GeS_4 tetrahedra, at 2.9 Å.

III. RESULT AND DISCUSSION

A. X-ray diffraction

1. Pair distribution functions

Figure 1 shows the pair distribution functions of Ge_xS_{100-x} ($x = 10, 20, 30, 33, 40$) glasses. The peaks in the pair distribution functions are compared to the interatomic distances in the crystals with the stoichiometric compositions ($x = 0$, 33, and 50): α-sulfur [34], the high-temperature phase of GeS_2 crystal [35], and GeS crystal [36–39]. The S-S bond length in a S_8 ring in α-sulfur is 2.06 Å [34]. The Ge-S bond length in GeS_4 tetrahedral unit in the high-temperature phase of GeS_2 crystal is 2.22 Å [35]. The Ge-S bond length in GeS crystal is 2.44 Å [37,39]. The first peaks, ranging from 1.8 to 2.8 Å, are attributed to these bonds. In $Ge_{30}S_{70}$ and $Ge_{33}S_{67}$, there is a small peak at 2.9 Å. This indicates the Ge-Ge distance in the edge-sharing tetrahedra (2.91 Å) [40]. The second peak, ranging from 3.1 to 4.0 Å, can be related to several types of inter-atomic distances. The second-neighbor S-S distance in S_8 ring molecules is estimated to be 3.34 Å, according to the bond length and the bond angle [34]. Even when an S_8 ring molecule opens to a helical chain, the second-neighbor distance can be preserved. The atomic correlations can contribute to the second peak in S-rich Ge-S glasses. The distance between neighboring S atoms in GeS_4 tetrahedron is estimated to be 3.62 Å, according the bond length and

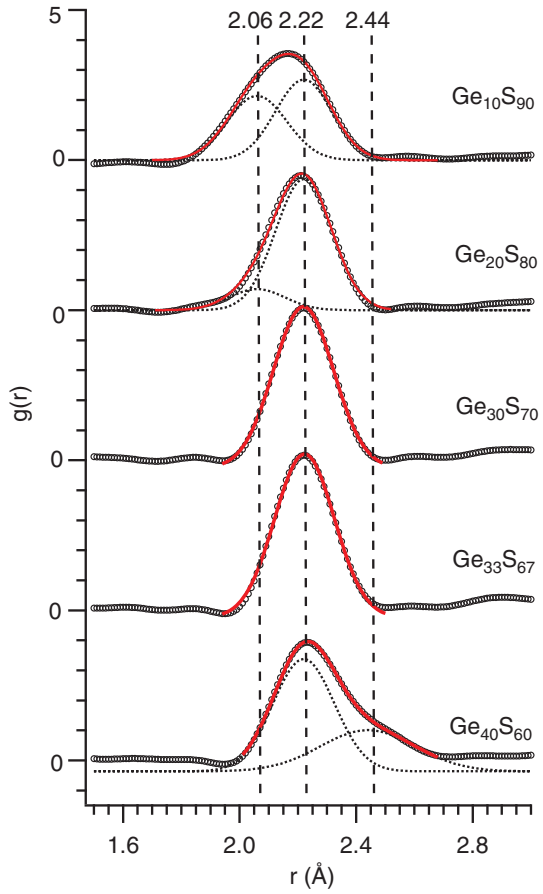

FIG. 2. The first peak in the pair distribution functions in Fig. 1 and the result of the curve fitting. Circles indicate the experimental data. The solid red curves indicate the fitted curves assuming one Gaussian or the sum of the two Gaussian curves. The dotted curves are the components of the Gaussian curves.

the bond angle [35]. The Ge-Ge distance in corner-sharing tetrahedra is 3.41 Å according to the simulations of glassy GeS_2 [40]. These atomic correlations impact on the second peak for all Ge compositions. Overall, the local structure obtained from the pair distribution functions is consistent with the previous picture on the structural transformation of molecularlike units, established by the Raman spectroscopy [13,41].

The detailed features of the first peak are shown in Fig. 2. The peak maximum position drastically shifts from 2.20 to 2.22 Å when Ge content changes from 10 to 20 at.% Ge. Also, a shoulder appears in the longer distance side around 2.40 Å at $x = 40$. These results indicate the local structural transformations at the composition changes from $x = 10$ to 20 and from $x = 33$ to 40.

For $x = 10$ and 20, there are two bond lengths to produce the first peak. One is the S-S bond in a S_8 ring in α-sulfur, or in polymeric sulfur chains. In both cases, the bond length is about 2.06 Å. The other bond is the Ge-S bond in a GeS_4 tetrahedron, which is formed in crystalline GeS_2 [35], and the bond length is 2.22 Å. The first peak is well fitted by the two Gaussian curves assuming the two types of bonds.

For $x = 30$ and 33, the first peak is fitted by only one Gaussian curve assuming the Ge-S bond in the GeS_4 tetrahedron. So far, a presence of Ge-Ge wrong bonds in GeS_2 glass ($x = 33$) was suggested as well as in $GeSe_2$ glass, forming S_3-Ge-Ge-S_3 ethanelike structure [15,41]. Indeed, the Ge-Ge bonds were observed in $GeSe_2$ glass from a neutron diffraction measurement by Salmon and Perti [42,43] and *ab initio* molecular-dynamics simulations by Cobb *et al.* [44], and a first-principles study on the Raman-active modes by Jackson *et al.* [45]. However, the amount of such Ge-Ge wrong bonds is supposed to be negligibly small in glassy GeS_2 according to x-ray and neutron diffraction measurements by Bytchkov *et al.* [30], the Ge *K*-edge extended x-ray absorption fine-structure spectroscopy (EXAFS) studies by Ibanez *et al.* [46] and Armand *et al.* [47], and *ab initio* molecular-dynamics simulations by Blaineau *et al.* [40,48]. These results are consistent with the present result of one Gaussian fitting.

For $x = 40$, the shoulder in the first peak indicates a presence of an additional bond site to the Ge-S bond in the GeS_4 tetrahedron. There are three possibilities. The first one is the longer Ge-S bond, which is formed in crystalline GeS [37,39]. In this case, Ge atoms are threefold coordinated. The bond length is 2.44 Å. The second one is the Ge-Ge bond, which appears as a S_3-Ge-Ge-S_3 ethanelike unit. According to the molecular dynamics simulations of GeS_2 glasses by Blaineau and Jund (2004) [48], the bond length is 2.42 Å although the content is very small in GeS_2 glasses. The last one is the Ge-Ge bond, which appears in amorphous germanium. The bond length is 2.46 Å [49,50]. So far, the Ge-Ge bond was assumed as the additional bond site in the EXAFS studies [46,47,51]. Bytchkov *et al.* assumed both the Ge-Ge bond and the longer Ge-S bond in their x-ray and neutron diffraction study [30]. However, according to the recent density functional/molecular dynamics simulations of $Ge_{42}S_{58}$ glasses by Akola *et al.* [52], the major bond types are the Ge-S bond with fourfold-coordinated Ge atoms (37%) and the Ge-S bond with threefold-coordinated Ge atoms (41%). Therefore, the two Ge-S bond sites (2.22 and 2.44 Å) were assumed in this study, and the first peak was well fitted as shown in Fig. 2.

The height of the Gaussian used for the fitting is plotted as a function of Ge content as shown in Fig. 3. This clearly indicates the transformation of the first-neighbor local structure in Ge-S glasses. For $x = 10$, the first peak is composed of Ge-S bonds and S-S bonds. With increasing Ge content, the contribution of the S-S bond decreases while that of the Ge-S bond increases. For $x = 33$, there is only the Ge-S bond. At $x = 40$, a longer Ge-S bond with 2.44 Å in length appears in addition to the Ge-S bond with 2.22 Å in length, belonging to the GeS_4 tetrahedron. Such changes in the local order must affect the electronic band structure. Figure 4 shows the schematic electronic band structure of glassy GeS_2 [53–55]. It should be pointed out that the energy splits into the bonding and antibonding levels by the formation of covalent bonds. The split energy becomes greater by forming a stronger (shorter) bond. Assuming that the energy of the lone-pair electrons is fixed, the energy gap E_g is determined by the split energy. For $x = 10$, there are the S-S bond (2.06 Å) and the Ge-S bond (2.22 Å). Considering that the total energy gap is determined by a *smaller* splitting (a *weaker* bond), the energy gap of

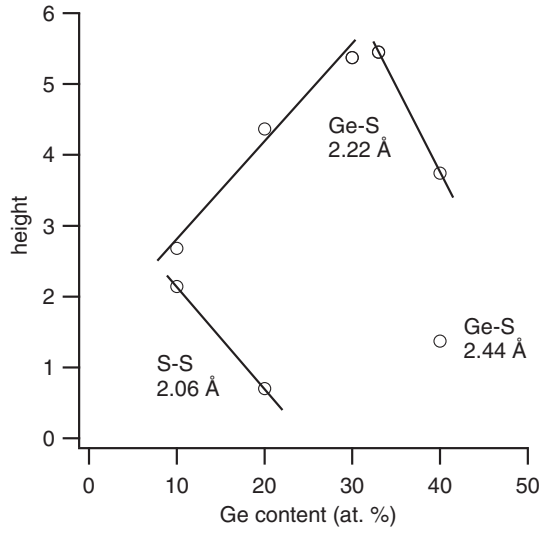

FIG. 3. Composition dependence of the peak heights obtained from the fitting in Fig. 2.

$Ge_{10}S_{90}$ is determined by the Ge-S bond. For $x = 33$, there is only Ge-S bond, and the energy gap of $Ge_{33}S_{67}$ is also determined by the Ge-S bond. However, for $x = 40$, a new contribution from longer (weaker) Ge-S bond appears. This longer (weaker) bond leads to a smaller split energy and, thus, E_g decreases when Ge content changes from $x = 33$ to 40. We compare this theoretical expectation with experimental data of the optical gap. Figure 5 shows the composition dependence of the optical gap and the optical absorption edge of Ge-S glasses [56–58]. (The optical absorption edge is determined by the wavelength where the absorption starts in the measured film, and it depends on the thickness of the film.) It is noted that the optical gap (optical absorption edge) moderately changes from $x = 10$ to 33, but it abruptly decreases from

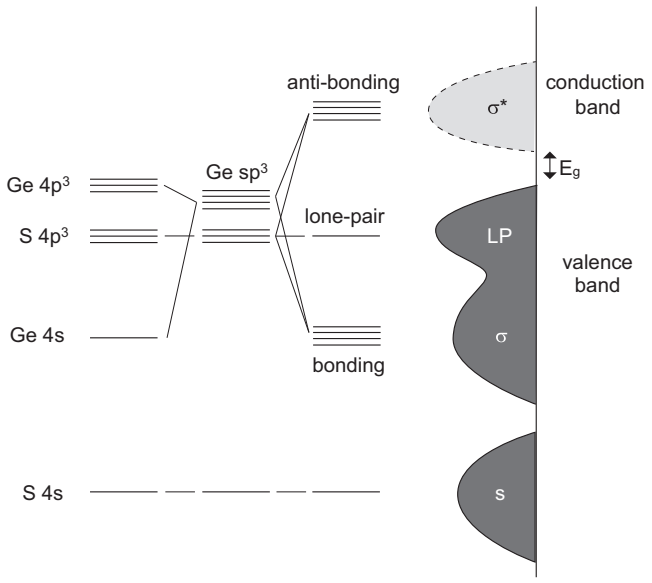

FIG. 4. Schematic diagram of the energy levels and the bands for glassy GeS_2.

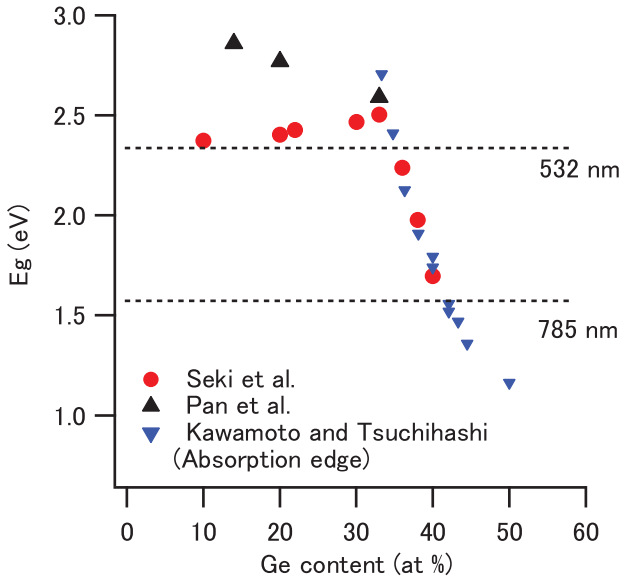

FIG. 5. Composition dependence of the optical gap of Ge-S glasses. Red circles indicate the data measured by Seki *et al.* [56] and the black triangles indicate the data measured by Pan *et al.* [57]. The optical absorption edges measured by Kawamoto and Tsuchihashi [58] are also shown in blue triangles. The broken lines indicate the energies of the excitation lasers used for Raman scattering measurement, which will be discussed in Sec. III B.

$x = 33$ to 40. This is exactly consistent with our expectation from the change in the local order. The result is also consistent with the visible color of Ge-S glasses, which is shown in Fig. 6. $Ge_{10}S_{90}$ and $Ge_{20}S_{80}$ color in yellow. $Ge_{30}S_{70}$ colors in orange with brown color, and $Ge_{33}S_{67}$ colors in yellow with a little orange. In essence, these colors are similar. However, the color of $Ge_{40}S_{60}$ drastically changes to be black. This

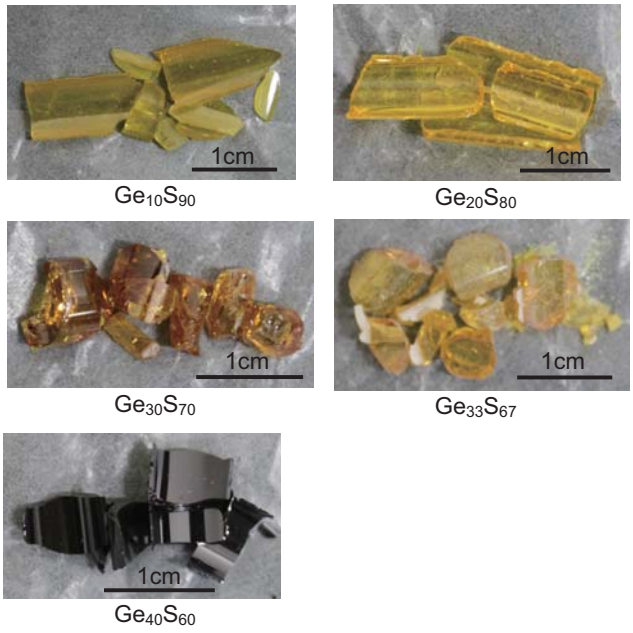

FIG. 6. Colors of Ge-S glasses.

TABLE I. Coordination numbers. The present results are indicated in bold. Previously published results are indicated in parentheses with the references. The error bars in the present results were estimated only from the maximum and minimum values of the x-ray weighing coefficients for partial structure factors W_{ij}, which depend on Q (see Appendix and Fig. 27). Other factors such as the accuracy in the determination of the pair distribution functions and the accuracy in the Gaussian fitting are not included in the evaluation of the errors. Reference [47]: Ge K-edge EXAFS; Ref. [64]: S K-edge EXAFS; Ref. [30]: x-ray and neutron diffraction; Ref. [52]: density functional/molecular dynamics simulations.

	S-S	Ge-S(I)	S-Ge(I)	Ge-S(II)	S-Ge(II)
$Ge_{10}S_{90}$	**1.21 ± 0.11**	**4.14 ± 0.56**	**0.45 ± 0.05**		
$Ge_{17}S_{83}$	(0.6 ± 0.2 [64])	(3.6 ± 0.4 [47])	(1.4 ± 0.2 [64])		
$Ge_{20}S_{80}$	**0.41 ± 0.07**	**4.48 ± 0.23**	**1.10 ± 0.06**		
	(0.3 ± 0.1 [64])	(3.6 ± 0.4 [47])	(1.7 ± 0.1 [64])		
$Ge_{30}S_{70}$		**3.73 ± 0.03**	**1.84 ± 0.02**		
$Ge_{31}S_{69}$		(3.9 ± 0.4 [47])			
$Ge_{33}S_{67}$		**3.77 ± 0.08**	**1.86 ± 0.04**		
	(0.01 [64])	(3.8 ± 0.4 [47])	(2.0 ± 0.1 [64])		
		(3.95 ± 0.15 [30])		(0.05 ± 0.15 [30]) (Ge-X)	
$Ge_{40}S_{60}$		**2.41 ± 0.12**	**1.58 ± 0.08**	**1.27 ± 0.06**	**0.85 ± 0.04**
		(2.7 ± 0.5 [47])	(2.0 ± 0.2 [64])	(0.9 ± 0.1 [47]) (Ge-Ge)	
		(2.72 ± 0.15 [30])		(1.16 ± 0.15 [30]) [Ge-X (X: S or Ge))	
$Ge_{42}S_{58}$		(2.37 ± 0.15 [30])		(1.52 ± 0.15 [30]) [Ge-X (X: S or Ge)]	
	(0.10 [52])	(3.24 [52])	(2.35 [52])	(0.32 [52]) (Ge-Ge)	

means that the optical gap abruptly decreases when Ge content changes from $x = 33$ to 40. The smaller energy gap can make a photosensitivity greater. In fact, we observed a particular photoinduced effect in amorphous $Ge_{46}S_{54}$ under air [59,60]. This change must be related to the specific electronic structure of Ge-rich Ge-S glasses, in other words, the appearance of a new longer bond in Ge-rich Ge-S glasses.

2. Coordination number

The coordination number can directly provide the picture of the network structure, and it is obtained from the radial distribution functions (RDF) (see Appendix). In general, there is a relationship between the RDF and the pair distribution functions $g(r)$ [61,62]:

$$\mathrm{RDF}(r) \equiv 4\pi r^2 \rho = 4\pi r^2 \rho_0 g(r), \tag{1}$$

where ρ_0 is an average number density of the system and $\rho_0 = N/V$ (N: the number of atoms in the system, V: the volume of the system). Figure 7 shows the RDF of Ge_xS_{100-x} glasses, and the coordination numbers calculated from the RDF are summarized in Table I. The structural picture of the network in each glass can be built up according to the coordination numbers as follows.

For $Ge_{30}S_{70}$ and $Ge_{33}S_{67}$, the first-neighboring atomic pair is only a Ge-S bond. The coordination number of S atoms around a Ge atom ($N_{\text{Ge-S(I)}}$) is about 4, forming a tetrahedron with four sp^3 hybrid orbitals. On the other hand, the coordination number of Ge atoms around a S atom ($N_{\text{S-Ge(I)}}$) is about 2. This simple case is illustrated in Fig. 8.

The GeS_4 tetrahedra are connected to each other, with either corner sharing (a) or edge sharing (b). According to the approximate *ab initio* molecular dynamics simulations [40], the Ge-Ge distance in the corner-sharing tetrahedra is 3.41 Å, while the Ge-Ge distance in the edge-sharing tetrahedra is 2.91 Å. In fact, there are small peaks at 2.9 Å in the RDFs of $Ge_{30}S_{70}$ and $Ge_{33}S_{67}$, which indicates the corner-sharing connection. Also, there are large peaks around 3.5 Å in the RDFs of $Ge_{30}S_{70}$ and $Ge_{33}S_{67}$ and the peak which originates from the edge-sharing connection at 3.4 Å is supposed to be included in the large peaks.

For $Ge_{20}S_{80}$, there are two types of bonds: Ge-S bond and S-S bond. $N_{\text{Ge-S(I)}}$ is about 4, indicating that all Ge atoms are surrounded by four S atoms, forming a GeS_4 tetrahedron. On the other hand, $N_{\text{S-Ge(I)}}$ is about 1 and the coordination number of S atoms around a S atom ($N_{\text{S-S}}$) is about $\frac{1}{2}$. In recent first-principles molecular-dynamics simulations of $Ge_{20}S_{80}$ (GeS_4) glasses by Bouzid *et al.* [65], $N_{\text{S-S}}$ is 1. Considering the electronic configuration of a sulfur atom, this result can be understood as follows. The uppermost orbital of a S atom is p orbital and there are four p electrons. Two of them are used for covalent bonds leaving two lone-pair electrons. Thus, S atoms have twofold coordination. $N_{\text{S-Ge(I)}} = 1$ and $N_{\text{S-S}} = 1$ mean that one side of a S atom is connected with a Ge atom and the other side is connected with a S atom. Therefore, GeS_4 tetrahedra can be connected forming S-S bond as shown in Fig. 9(a). However, $N_{\text{S-S}}$ is $\frac{1}{2}$ in the present experiment. This means that a half of S-S bonds are broken, forming dangling bonds as illustrated in Fig. 9(b). It is well known that electron spin resonance (ESR) signals are not detected in chalcogenide glasses in general, and this is explained by the change from the uncharged paramagnetic center with an unpaired electron (D^0) to the positively and negatively charged diamagnetic defect centers (D^+ and D^-) [66,67]. However, germanium sulfide

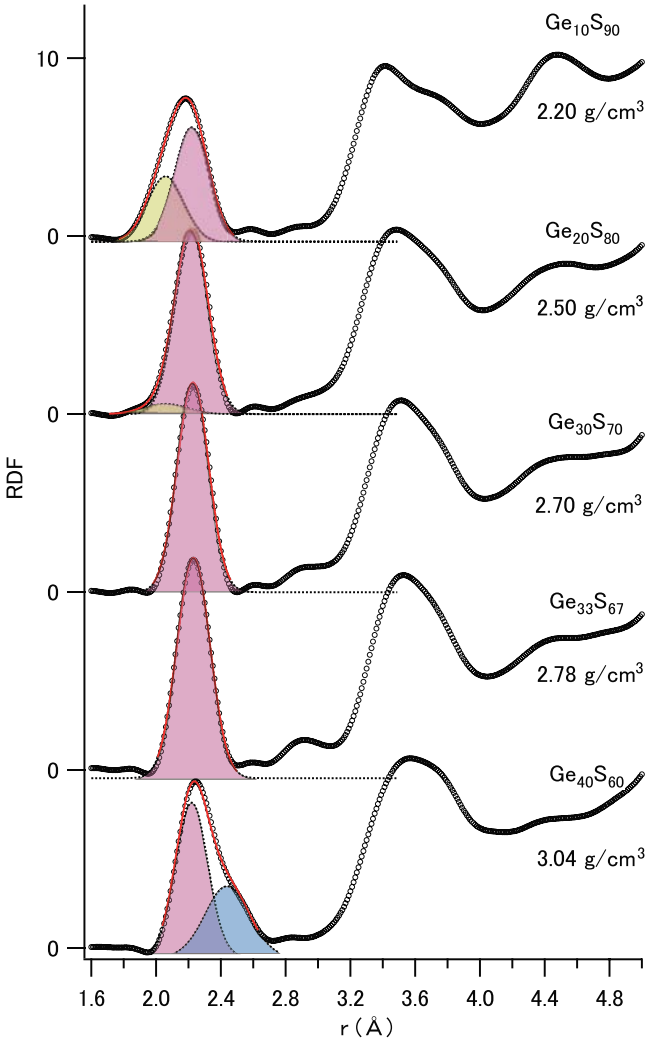

FIG. 7. Radial distribution functions (RDF) of Ge-S glasses. The mass densities in the literature [63] were used to obtain the RDF. The areas for the estimation of the coordination number are indicated in different colors: S-S (yellow), Ge-S (I) (pink), and Ge-S (II) (light blue).

glasses are exceptional, and clear ESR signals are detected [68–73]. Especially, Černý and Frumar [72] suggested from their ESR results that the defects were created by the S-S bond breaking between two GeS_4 tetrahedra and this agrees with the structural model illustrated in Fig. 9(b). Using the structural picture, the result of the simulations by Bouzid *et al.* ($N_{S\text{-}S} = 1$) can be understood as the ideal case of no structural defects, which was probably realized by a specific quench condition. It is noted that a series of GeS_4 tetrahedra in Fig. 9(b) indicates a chainlike (one-dimensional) connection and that this is different from three-dimensional network in GeS_2 (Fig. 8). Thorpe [7] and Phillips [6] predicted that the S-rich Ge-S glasses have a *floppy* nature, considering that twofold-coordinated S atoms are dominant in the glasses. Probably, polymeric S-S chains could be regarded as the *floppy* chains. However, our model requires a modification on the structural units of the *floppy* chains from -S- to -S-Ge-S-, or GeS_4 tetrahedra.

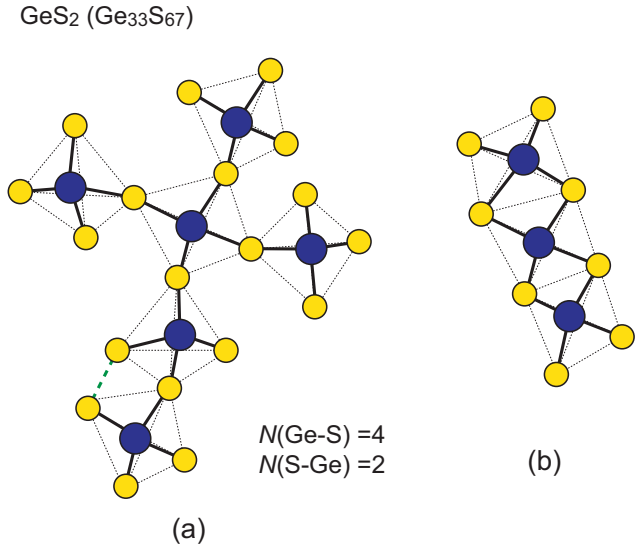

FIG. 8. Schematic illustration of the possible network structure of GeS_2 ($Ge_{33}S_{67}$) glasses. (a) Network connection with corner-sharing GeS_4 tetrahedra, (b) network connection with edge-sharing GeS_4 tetrahedra. The green broken line indicates a possible position where a S-S bond of the edge dimer in "outrigger raft" can be formed.

For $Ge_{10}S_{90}$, there are also two types of bonds: Ge-S bond and S-S bond. $N_{Ge\text{-}S(I)}$ is about 4, indicating that all Ge atoms are surrounded by four S atoms, forming a GeS_4 tetrahedron. On the other hand, $N_{S\text{-}Ge(I)}$ is $\frac{1}{2}$, and $N_{S\text{-}S}$ is about 1.25. These coordination numbers can be explained by the model shown in Fig. 10. In the model, $Ge_{10}S_{90}$ glasses are replaced to $Ge_{11}S_{89}$, which is equivalent to GeS_8. A GeS_8 unit consists of a GeS_4 tetrahedron and four S atoms attached to the four ends of the tetrahedron, forming $Ge(S\text{-}S)_4$. Two of the ends of a GeS_8 unit connect with the end of another GeS_8 unit, forming polymeric chains. The remaining two ends of the GeS_8 unit are supposed to be dangling bonds because $N_{S\text{-}S}$ is about 1.25 $[(1 \times 2 + 2 \times 2 + 1 \times 4)/8]$. Regarding the dimensionality of the network connection, $Ge_{33}S_{67}$ and $Ge_{33}S_{67}$ have three-dimensional character, $Ge_{20}S_{80}$ and $Ge_{10}S_{90}$ have one-dimensional one (chainlike connection).

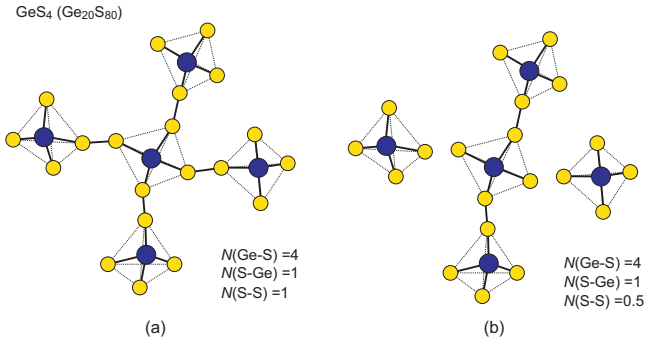

FIG. 9. Schematic illustration of the possible network structure of GeS_4 ($Ge_{20}S_{80}$) glasses. (a) network connection with complete (no-sharing) GeS_4 tetrahedra (b) chain-like (one-dimensional) connection with complete (no-sharing) GeS_4 tetrahedra.

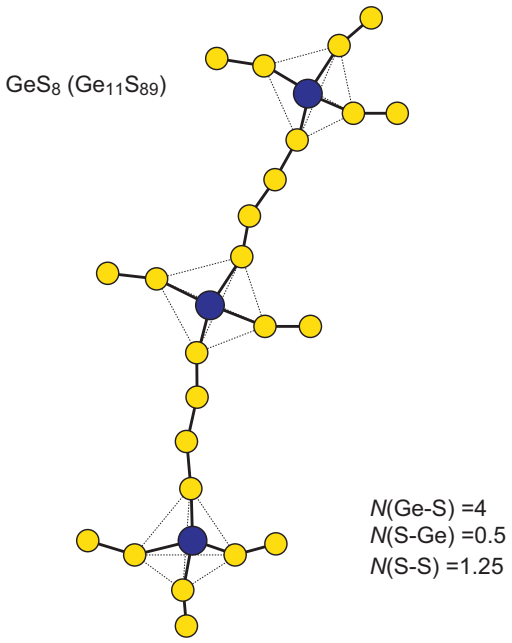

FIG. 10. Schematic illustration of the possible network structure of GeS_8 ($Ge_{11}S_{89}$) glasses. GeS_8 units connect to each other to form *floppy* network.

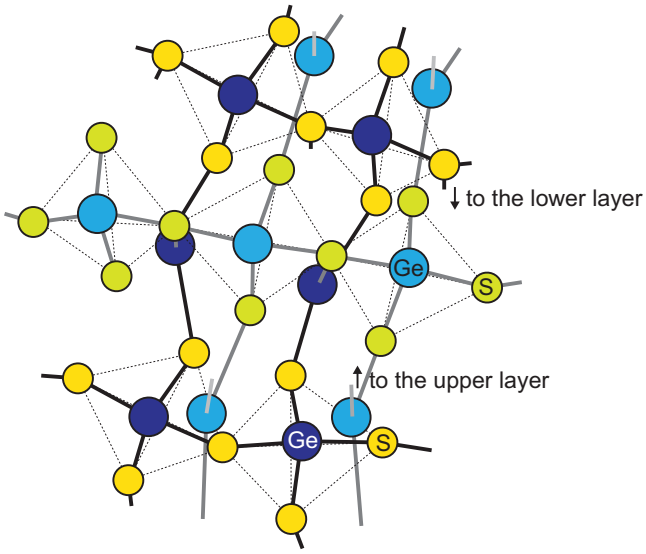

FIG. 11. Schematic illustration of a possible network structure of $Ge_{40}S_{60}$ glasses. A series of GeS_4 tetrahedra and their *bridges* made of the azure Ge atoms and the lime S atoms form the upper layer, while that made of the navy blue Ge atoms and the yellow S atoms form the lower layer. Both of the layers are bonded to each other, with threefold-coordinated atoms.

The network is supposed to be flexible (*floppy*) with decreasing the dimensionality from three to one. In fact, the Vickers hardness rapidly decreases with increasing S content for glasses with 33 at.% Ge to 10 at.% Ge [58]. The glass transition temperature and the softening temperature rapidly decrease with increasing S content for glasses with 33 at.% Ge to 10 at.% Ge [58,74]. The average thermal expansion coefficient in the temperatures between room temperature and the glass transition temperature rapidly increase with increasing S content for glasses with 33 at.% Ge to 10 at.% Ge [58]. These physical and thermal properties agree with the expectation of the floppy nature in the S-rich Ge-S glasses.

For $Ge_{40}S_{60}$ glass, two types of the Ge-S bond mainly contribute to construct the network system as shown in the previous section. One Ge-S bond [Ge-S(I)] is shorter with 2.22 Å in length and the Ge atom is fourfold coordinated. The sp^3 hybrid orbitals are supposed to be formed in the Ge atom. The other Ge-S bond [Ge-S(II)] is longer with 2.44 Å in length and the Ge atom is threefold coordinated. This picture coincides with our previous model for Ge-rich Ge-S (Se) glasses. In the model, we assumed the fragments of the double layer in crystalline GeS. The double layer is built up with threefold-coordinated Ge atoms and threefold-coordinated S atoms. Two *p* orbitals of both Ge and S atoms are supposed to participate in covalent bonding, and zigzag Ge-S chains are formed. In addition, one empty orbital of a Ge atom and one lone-pair orbital of a S atom form a coordinate bond, whose direction is perpendicular to the zigzag chains. In this way, "double layer" is formed [16]. Figure 11 is a possible network model of $Ge_{40}S_{60}$ glasses. The network is composed of layers, and each layer is composed of the sequences of GeS_4 tetrahedral units and the Ge atoms which bridge two tetrahedra. The Ge atoms bridge again one tetrahedron on the adjacent layer, forming threefold coordination. In the model, the *local* coordination numbers are $N_{\text{Ge-S}} = 4$, $N_{\text{S-Ge}} = 2$ (tetrahedron); $N_{\text{Ge-S}} = 3$, $N_{\text{S-Ge}} = 3$ (double layer). The *averaged* coordination numbers were estimated by assuming the two types of the Ge-S bond as shown in Table I. In Fig. 11, there are two types of Ge atoms (fourfold coordinated and threefold coordinated), and two types of S atoms (twofold coordinated and threefold coordinated). In both of the atoms, the former one is categorized into the tetrahedral unit type, and the latter one is categorized into the double-layer type. In Fig. 11, the ratio of these is 1:1. However, the ratio can be changed by by breaking a bond or by inserting a Ge-Ge or S-S wrong bond. Assuming that the ratio is 6:4, $N_{\text{Ge-S(I)}} = 4 \times 0.6 + 0 \times 0.4 = 2.4$, $N_{\text{Ge-S(II)}} = 0 \times 0.6 + 3 \times 0.4 = 1.2$, $N_{\text{S-Ge(I)}} = 1 \times 0.6 + 2 \times 0.4 = 1.4$, and $N_{\text{S-Ge(II)}} = 1 \times 0.6 + 1 \times 0.4 = 1.0$. These are in good agreement with the coordination numbers estimated from the present result, listed in Table I. It is noted that the weaker Ge-S bonds characterize the network structure in terms of rigidity. Vickers hardness increases a little, showing that the network becomes more *rigid* with increasing Ge content from 33 at.% Ge to 44 at.% Ge [58]. On the other hand, the glass transition temperature and the softening temperature decrease with increasing Ge content from 33 at.% Ge to 44 at.% Ge [58,74]. The viscosity at the same temperature also decreases with increasing Ge content [75]. These results seem to show that the glasses become more *floppy* in the Ge-rich region to the contrary. However, these features can be understood as the increase of the rigidity in the Ge-rich region at *room temperature* due to the participation of the new longer Ge-S bonds, and the breakage of the Ge-S bonds at *high temperatures* due to the weakness of the bonds.

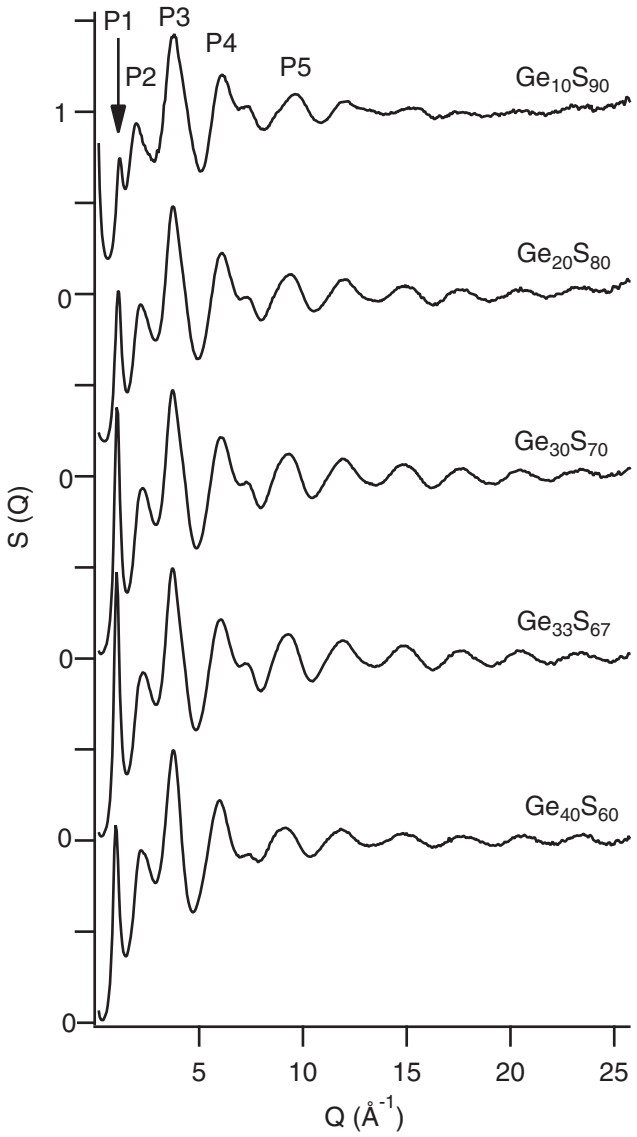

FIG. 12. Structure factors of Ge_xS_{100-x} ($x = 10, 20, 30, 33, 40$) glasses.

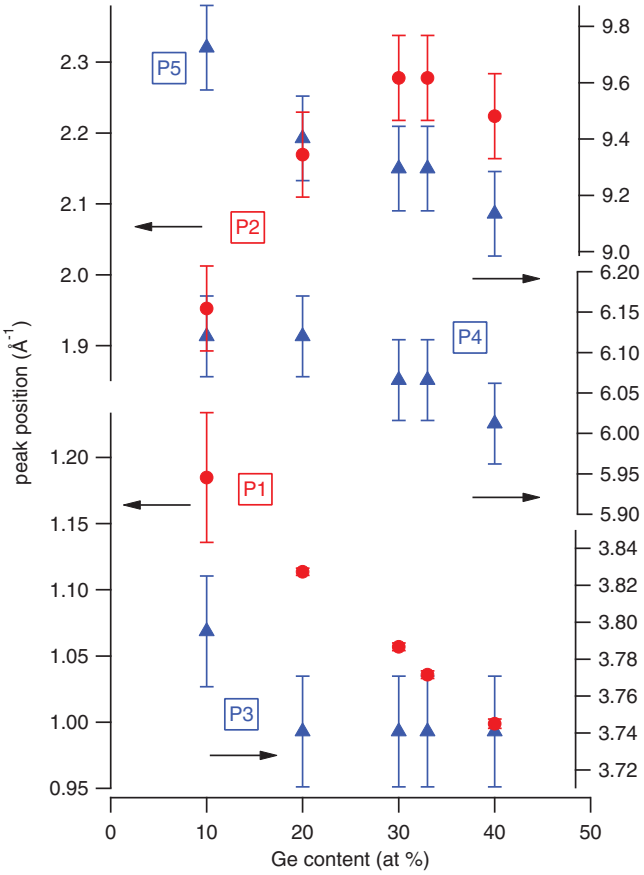

FIG. 13. Composition dependence of the peak positions in the structure factors of Ge_xS_{100-x} ($x = 10, 20, 30, 33, 40$) glasses. P1, P2, P3, P4, and P5 are indicated in Fig. 12.

3. Structure factors

The structure factors reflect the structural transformation in various spatial ranges, short-range, medium-range, and nanoscopic scale, and the changes in the reciprocal space are sometimes much more clearly observed than those in the real space. Figure 12 shows the structure factors of Ge_xS_{100-x} ($x = 10, 20, 30, 33, 40$) glasses in 0.16 Q 25.78 $Å^{-1}$. It is noted that a clear oscillation is observed up to 25 $Å^{-1}$ for each compound, showing that the measurement has been made very precisely using the intensive x-ray source whereas the atomic form factors decrease with increasing Q. Basic features are similar to those of the previous x-ray diffraction result measured by Fueki *et al.* [28] except the result of $Ge_{10}S_{90}$. In their result, the first peak almost disappears and the second peak is larger than the present result. The neutron diffraction pattern of GeS_2 ($Ge_{33}S_{67}$) [76,77] is also similar to the present data. (The first peak in the data of Lin *et al.* [76] is a little bit larger.) The structure factors of $Ge_{33}S_{67}$ and $Ge_{40}S_{60}$ measured by Bytchkov *et al.* up to 20 $Å^{-1}$ [30] have also similar profile to the present result.

Figure 13 shows the composition dependence of the peak positions in the structure factors of Ge_xS_{100-x} ($x = 10, 20, 30, 33, 40$) glasses. As shown in the figure, the position of each peak changes with increasing Ge content: some of them monotonously decrease (increase), and some of them have an onset composition of the change. Figure 14 shows the composition dependence of the peak height in the structure factors of Ge_xS_{100-x} ($x = 10, 20, 30, 33, 40$) glasses. The peak height does not change so much except for P1.

The first peak in the structure factors is often referred as "first sharp diffraction peak (FSDP)," and indicates medium-range order [67,78]. In the previous studies [79] it has been accepted that the FSDP displays the spacing in layerlike structure in the materials. However, nowadays it is widely accepted that the FSDP suggests the chemical ordering of interstitial voids in the network of glasses [80–82] or the periodicity arising from the boundaries between a succession of the cages which comprise the structure of a three-dimensional covalent network [83,84]. Recently, Crupi *et al.* proposed the periodicity of the boundaries of voids in a random network as the origin of the FSDP [85]. In any case, these authors note

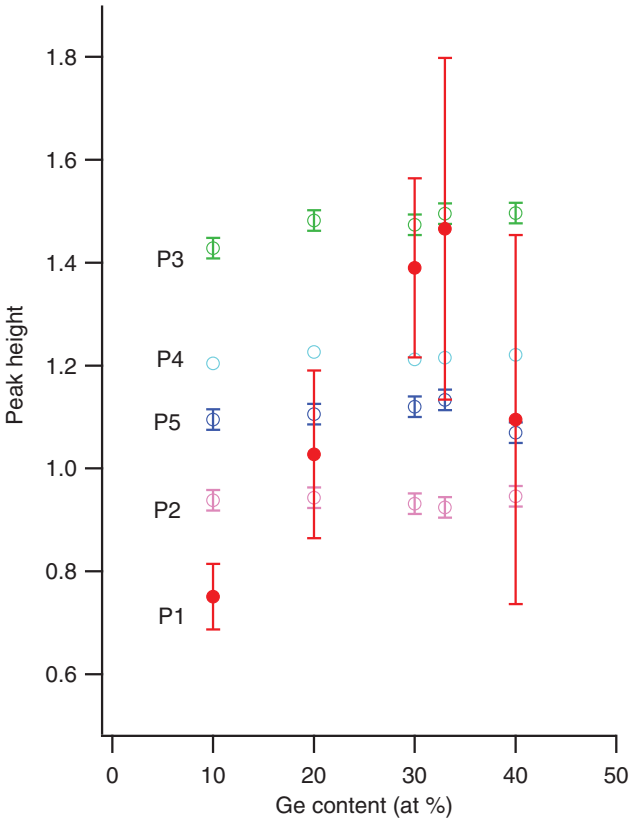

FIG. 14. Composition dependence of the peak height in the structure factors of Ge_xS_{100-x} ($x = 10, 20, 30, 33, 40$) glasses.

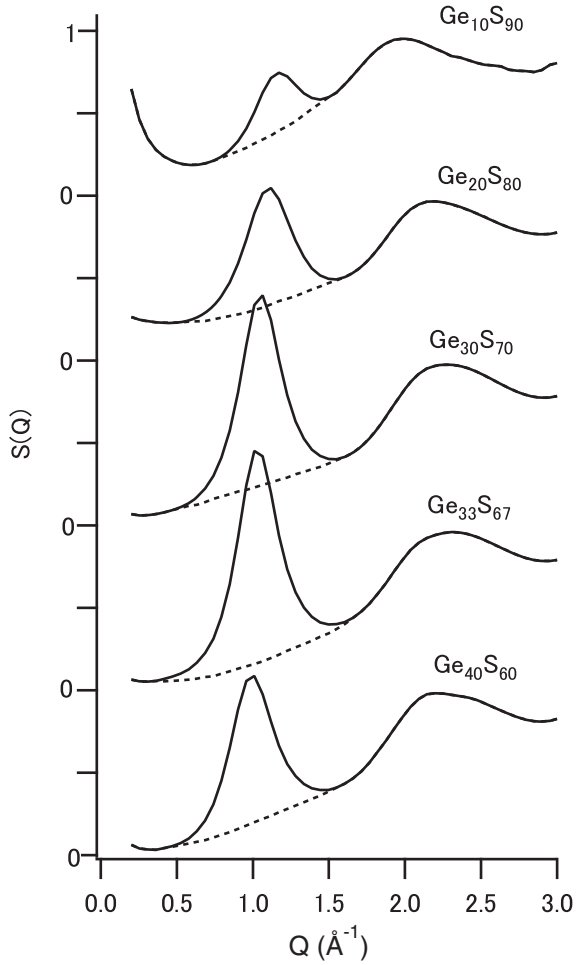

FIG. 15. Structure factors around the FSDP of Ge_xS_{100-x} ($x = 10, 20, 30, 33, 40$) glasses. The broken curves are artificially produced structure factors assuming that there is no FSDP.

on the spatial distribution where no atoms exist because of a sort of "frustration" in the atomic arrangement in amorphous materials and tried to express the characteristic distance of the spatial distribution according to their theory. To confirm the validity of the understanding, we examined how the FSDPs affect the pair distribution functions by assuming the structure factors without the FSDP (the broken curves in Fig. 15). Figure 16 shows the pair distribution functions obtained from the structure factors *with* and *without* the FSDP. As shown in the figure, the difference appears at the distance from 4 to 5.5 Å. In the spatial range, the pair distribution functions obtained from the structure factors *with* the FSDP is *smaller* than those obtained from the structure factors *without* the FSDP. The difference is the greatest at 30 and 33 at.% Ge, where the FSDP has a maximum height (Fig. 14). The less pair distribution functions mean the less relative atomic distribution. In other words, there can be voids in the network. The spatial range is consistent with a value roughly estimated from the peak position using $2\pi/Q_1$ (Q_1: the peak position of the FSDP): 5.3–6.3 Å.

Figure 13 shows that the position of the FSDP decreases with increasing Ge content. This suggests that the spatial distribution of the network cages with voids becomes larger with increasing Ge content. At 30 and 33 at.% Ge, two separated GeS_4 tetrahedral units are connected by another GeS_4 tetrahedron, and an interstitial void is produced between the tetrahedra [Fig. 8(a)]. The *bridging* tetrahedron plays roles in connecting the other tetrahedra, and in keeping a distance between them as if it is a *prop*. When Ge content changes from 33 at.% Ge to 40 at.% Ge, a new Ge atom is added to bridge a gap between two GeS_4 tetrahedra, forming weaker (longer) Ge-S bonds (Fig. 11). Since the occupied volume by the bridging atoms becomes smaller (a GeS_4 tetrahedron $\rightarrow$ a S-Ge-S unit), and the bond length becomes longer, the interstitial void is supposed to be larger. This is consistent with the experimental result of the FSDP position. On the other hand, in S-rich region, S atoms are inserted between the GeS_4 tetrahedra. It is noted, in general in sulfur molecules, that S atoms bond to each other, fixing a bond length, a bond angle, and a dihedral angle, but the sign of the dihedral angle can be changed flexibly [86]. This would reduce props between two GeS_4 tetrahedra and the interstitial void is expected to be smaller. This is also consistent with the result of the FSDP position. In Fig. 14, the peak height has a maximum at 33 at.% Ge. The peak height may be related to a sharpness of the peak, and the sharpness can be evaluated by a peak width. The peak width was determined by a curve fitting assuming Lorentzian and Gaussian as shown in Fig. 17. Here, we used a net FSDP curve by subtracting a base curve (the broken curve in Fig. 15) from the experimental curve. According to the discussion on

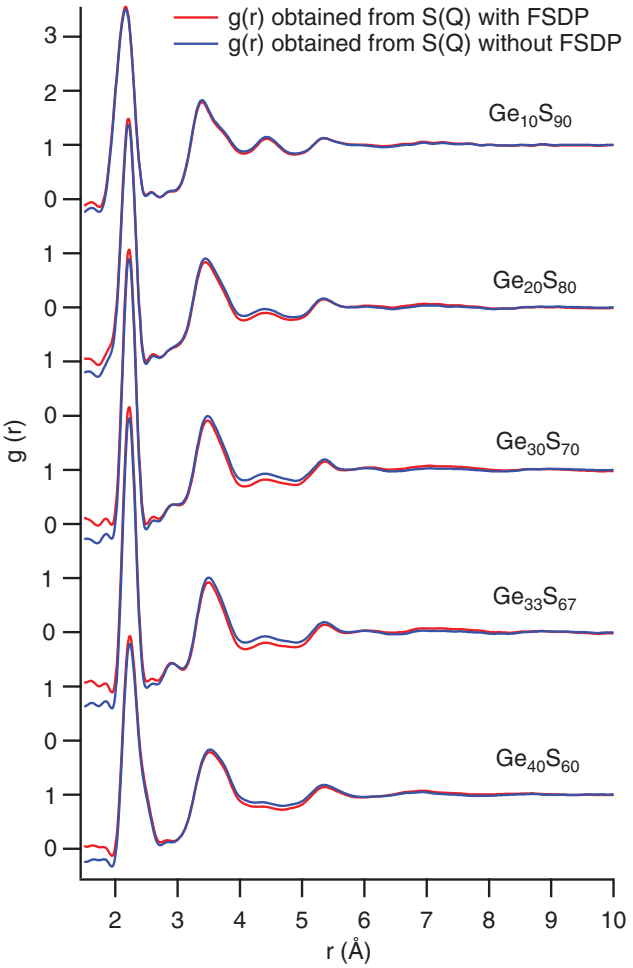

FIG. 16. Pair distribution functions obtained from the structure factors *with* the FSDP (the experimental data: red) and without the FSDP (artificially produced data: blue).

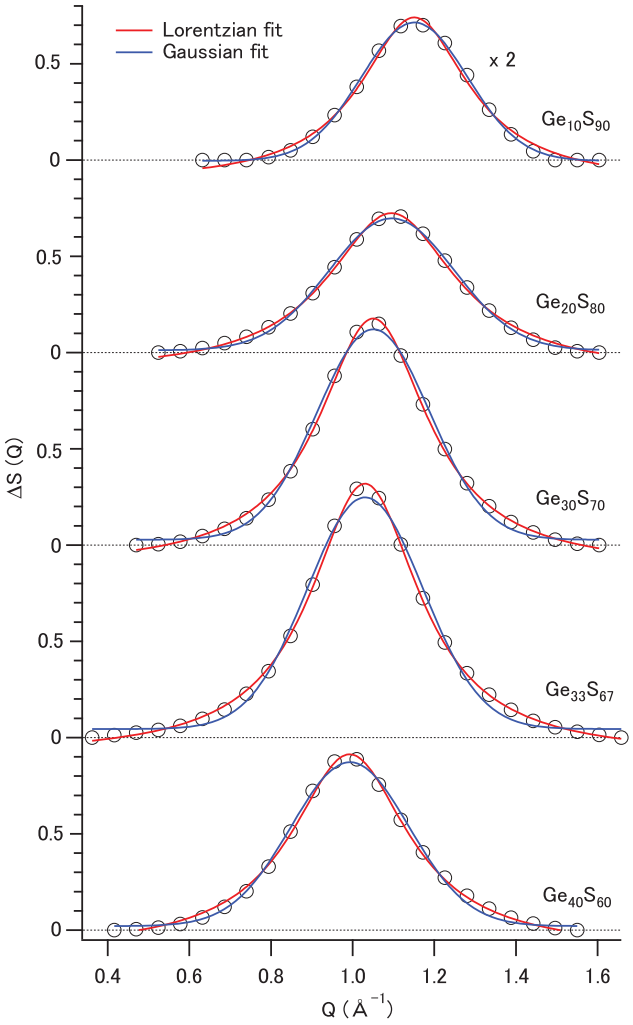

FIG. 17. Curve fitting to the net FSDP curve using the Lorentzian and Gaussian. The net FSDP curves were obtained by subtracting the base curve (the broken curve in Fig. 15) from the experimental curve in Fig. 15. The curve for $Ge_{10}S_{90}$ is multiplied by 2.

the curve fit to the FSDP for vitreous silica by Wright *et al.* [87], the Gaussian fit is very poor, and the low-Q side of the peak is very closely Lorentzian: the high-Q side is not fitted well even with Lorentzian. In this study, the Lorentzian is in a good agreement with the net FSDP. The Gaussian fit is also close to the net FSDP curve, although the Lorentzian fit looks better. Good Lorentzian fit would mean that the size distribution of the voids is narrow to induce *resonance* because Lorentzian is derived from a resonant phenomenon. The peak width w may be defined in the Lorentzian form

$$y = y_0 + A\frac{w^2}{(x - x_0)^2 + w^2}. \tag{2}$$

When $y_0 = 0$, y is the half of the maximum at $x = x_0 \pm w$. The corresponding width may be defined in the Gaussian form

$$y = y_0 + A\exp\left[-\frac{(x - x_0)^2}{2w^2}\right]. \tag{3}$$

When $y_0 = 0$, y is $\exp(-0.5) = 0.61$ at $x = x_0 \pm w$. The composition dependence of the peak width is shown in Fig. 18. The result indicates that the size distribution of the void is narrowest at 33 at.% Ge, in other words, GeS_4 tetrahedra are the most uniformly packed at 33 at.% Ge. It is noted that the peak becomes narrower again at 10 at.% Ge. This is probably due to the appearance of a new type of the network connection at 10 at.% Ge. In fact, the Gaussian fit is more appropriate than the Lorentzian fit at 10 at.% Ge. More flexible one-dimensional chains (Fig. 10) may produce more uniformly packed network system. Or, the introduction of S_8 ring molecules in the S-rich region, which will be discussed in details in Sec. III A 5, may affect the packing conditions in the network system.

4. Small-angle x-ray scattering

In Fig. 15, there is a large increase in the structure factors at the small-angle region for $Ge_{10}S_{90}$. The composition dependence of the structure factors at the fixed low Q is shown in Fig. 19. The structure factors at the small-angle region increase with decreasing Ge content, and they are the maximum at 10 at.% Ge in this study. Such large small-angle scattering was also observed in the small-angle neutron

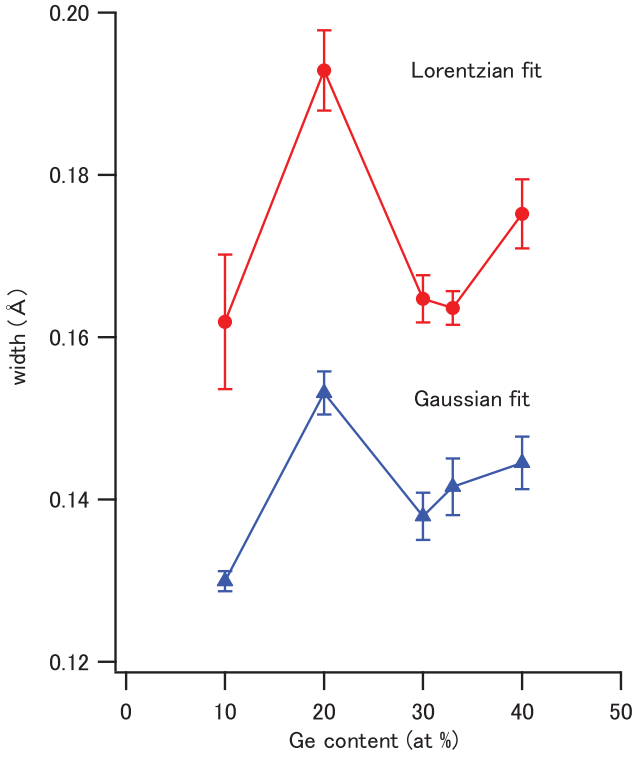

FIG. 18. Composition dependence of the width of the FSDP, obtained from the Lorentzian (red circles) and the Gaussian (blue triangles) fit.

scattering measured by Bychkov *et al.* [29]. According to their result, the intensity changes with time. The large small-angle scattering suggests a presence of large-scale order in nanoscopic scale. Details of the large-scale order will be discussed in Sec. III B.

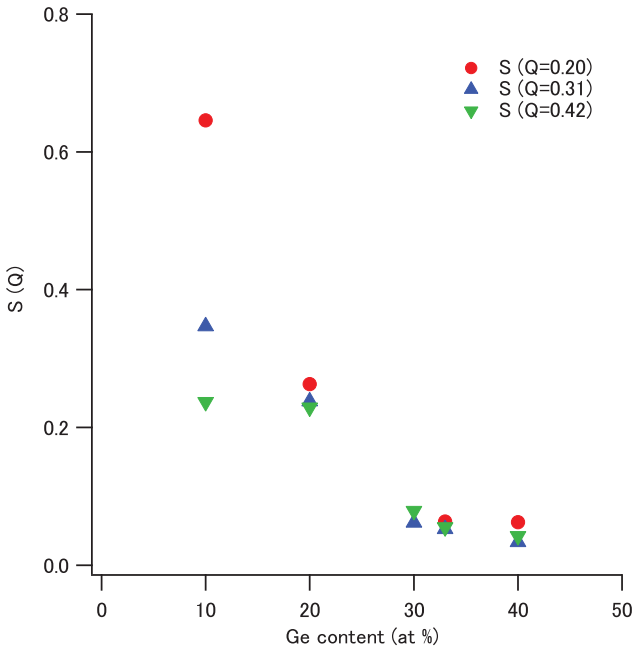

FIG. 19. Composition dependence of the structure factors S (Q) at the fixed low Q.

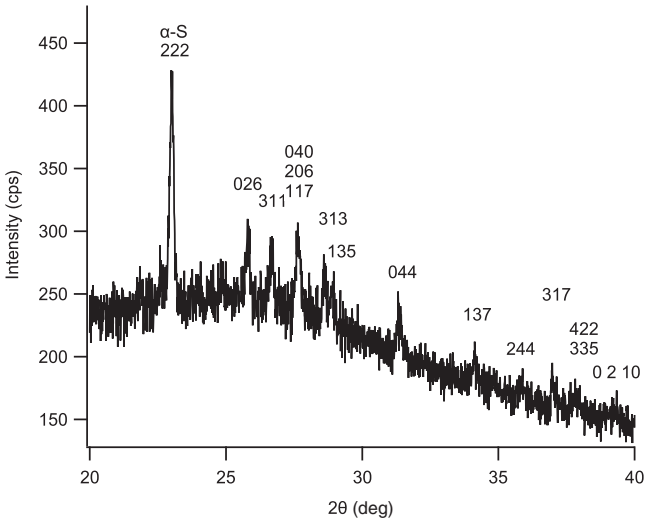

FIG. 20. Powder diffraction pattern of $Ge_{10}S_{90}$ using a conventional x-ray diffractometer with Cu K_α x-ray source (Rigaku RINT2000).

5. *Powder x-ray diffraction*

In the first XRD measurement of $Ge_{10}S_{90}$, several "spikes," indicating Bragg peaks from crystals, were observed in the Q range from 1.6 to 2.1 $Å^{-1}$. However, in the second measurement using another part of the sample, such spikes were not observed. Since the Q resolution of the diffractometer on BL04B2 at SPring-8 is optimized for the measurement of disordered materials, the diffraction peaks from the crystals could not be detected well with the diffractometer. Therefore, powder x-ray diffraction measurement of $Ge_{10}S_{90}$ was carried out using a conventional x-ray diffractometer with Cu K_α x-ray source (Rigaku RINT2000). The diffraction pattern is shown in Fig. 20. Obviously, there is α sulfur, which is composed of S_8 ring molecules, in $Ge_{10}S_{90}$. Kawamoto and Tsuchihashi [58] investigated the amount of S_8 ring molecules in Ge_xS_{100-x} (10 x 33) glasses by extracting S_8 ring molecules with CS_2. According to their result, there are S_8 ring molecules in S-rich Ge_xS_{100-x} glasses ($x < 20$). This is consistent with the present result of the powder x-ray diffraction. The large small-angle x-ray scattering in $Ge_{10}S_{90}$ glasses can be related to amorphous phase/crystalline phase co-existence. Details of the phase separation will be discussed in Sec. III B.

B. Raman spectra

1. *Composition dependence of building blocks in the network structure*

The network structure of Ge_xS_{100-x} glasses has been mainly investigated by Raman spectra. Our structural models, obtained from x-ray diffraction, can be reviewed, by comparing with the Raman spectra. Figure 21 shows the Raman spectra of Ge_xS_{100-x} glasses using the excitation laser

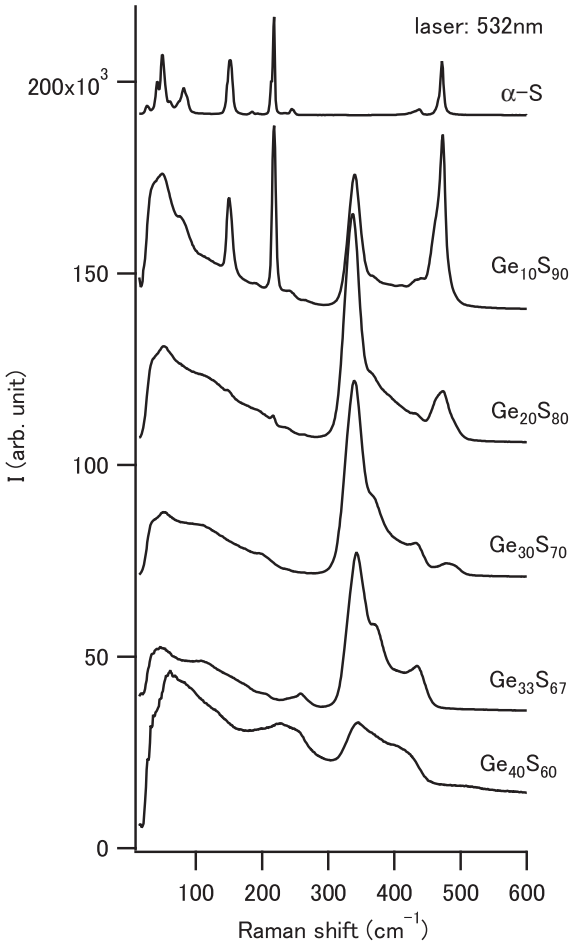

FIG. 21. Raman spectra of Ge_xS_{100-x} ($x = 10$, 20, 30, 33, 40) glasses using the excitation laser with the wavelength of 532 nm.

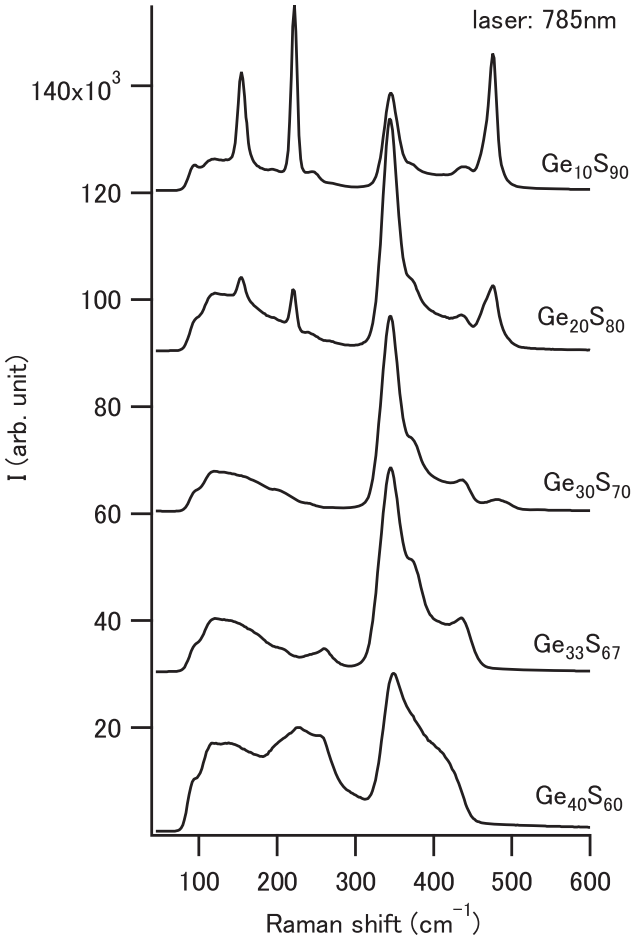

FIG. 22. Raman spectra of Ge_xS_{100-x} ($x = 10$, 20, 30, 33, 40) glasses using the excitation laser with the wavelength of 785 nm.

with the wavelength of 532 nm and Fig. 22 shows the Raman spectra using the excitation laser with the wavelength of 785 nm. In the measurement using the 532-nm excitation laser, a narrow notch filter was used to eliminate a strong Rayleigh line and the spectrum was measured in the low-frequency region up to 50 cm^{-1}. On the other hand, in the measurement using the 785-nm excitation laser, the background from the Rayleigh line was very strong and a short-pass sharp cut filter was used, instead of a notch filter. Because of this reason, the observable lowest frequency became greater to be 90 cm^{-1}. The Raman spectra obtained by the 532-nm laser excitation is consistent with previous results measured by Sugai (514.5 nm) [14], Kotsalas and Raptis (488 nm) [88], and Takebe *et al.* (514.5 nm) [63]. The result ensures that the samples in the present experiment were properly prepared. The Raman spectra obtained by the 785-nm laser excitation is a little bit different from those obtained by the 532-nm laser excitation. The spectrum of $Ge_{40}S_{60}$ glasses obtained by the 785-nm laser excitation has a smaller background component and has larger peaks in 200−300 cm^{-1} and 320−450 cm^{-1}. The feature of the peaks is the same as that in the spectrum obtained by the 799.3-nm krypton laser excitation measured by Lucovsky *et al.* [15], and that obtained by the 632.8-nm He-Ne laser excitation measured by Yamaguchi *et al.* [89]. Considering that the optical gap rapidly decreases from 2.5 eV (496 nm) to 1.6 eV (775 nm) as increasing the Ge composition from 33% to 40% (Fig. 5), the enhancement of those peaks is attributed to a resonant Raman scattering. The peaks at 150 and 220 cm^{-1} are larger in the spectrum of $Ge_{20}S_{80}$ glasses obtained by the 785-nm laser excitation than in the spectrum obtained by the 532-nm laser excitation. Such larger peaks are also observed in the spectrum obtained by 625-nm laser excitation measured by Lucovsky *et al.* [13].

In Table II, Raman-active modes in Ge_xS_{100-x} glasses are summarized. The breathing mode of the corner-sharing tetrahedron appears at 342 cm^{-1} [94,95] and the peak is observed throughout the whole composition range. This is consistent with our network models (Figs. 8–11), suggesting that the tetrahedral units are the main components to build up the network in the glasses throughout the entire composition range. The peak at 375 cm^{-1} is referred as the companion A_1^c peak, and is assigned as the vibrational mode of the edge-sharing GeS_4 tetrahedra [14]. The peak is observed in the spectra of $Ge_{30}S_{70}$ and $Ge_{33}S_{67}$ and this coincides with the present result of the pair distribution functions of $Ge_{30}S_{70}$ and $Ge_{33}S_{67}$ (Fig. 1). As we mentioned, the peak at 2.9 Å indicates the Ge-Ge distance in the edge-sharing GeS_4 tetrahedra [40].

TABLE II. Raman-active modes of Ge-S glasses. AsyBBend: antisymmetric bond bending; SyBBend: symmetric bond bending; SyBStr: symmetric bond stretching.

Molecular unit	Mode	Frequency (cm^{-1})	Reference
S_8 (AsyBBend)	A_1	150	[90]
S_8 (SyBBend)	A_g	220	[90]
S_8 (SyBStr)	A_g	472	[90]
S_μ (helical chain)		461	[91–93]
GeS_4 (corner sharing)	A_1	342	[94,95]
GeS_4 (edge sharing)	A_1 (A_1^c)	375	[14]
S-S (outrigger raft)		443	[41,96]
S_3Ge-GeS_3		240	[15]
S_3Ge-GeS_3	A_{1g}	340	[15]
S_3Ge-GeS_3		376	[15]
GeS	A_g	250	[39]

In the Raman spectra of S-rich glasses, $Ge_{10}S_{90}$ and $Ge_{20}S_{80}$, there are sharp peaks at 150, 220, and 472 cm^{-1}. These peaks are associated with S_8 ring molecules, and observed in the Raman spectra of α sulfur (crystal) [90] and liquid sulfur [91,92,97]. The presence of S_8 ring molecules in $Ge_{10}S_{90}$ was confirmed by a S_8 ring extraction experiment performed by Kawamoto and Tsuchihashi [58]. The powder x-ray diffraction pattern of $Ge_{10}S_{90}$ glasses in Fig. 20 also supports that there are S_8 ring molecules (sulfur crystals) in $Ge_{10}S_{90}$ glasses. The ring molecules would be isolated from the network in the glasses because there is no room to connect with other atoms in the *closed* molecules. However, the crystal in $Ge_{10}S_{90}$ is *not* exactly the same as that in α sulfur. Figure 23 shows Raman spectra of α sulfur and $Ge_{10}S_{90}$, ranging from 120 to 250 cm^{-1}. The peaks originated from α sulfur are broadened in $Ge_{10}S_{90}$. In addition, there are sharp peaks in the frequency region lower than 100 cm^{-1}, which are assigned to the phonon modes, in the Raman spectrum of α sulfur in Fig. 21, while the corresponding peaks are quite broadened and overlap to each other in the Raman spectrum of $Ge_{10}S_{90}$. Therefore, the sulfur crystals in $Ge_{10}S_{90}$ are considered not to be the same as pure α sulfur, and are distorted kind of amorphous form. The details will be discussed again in the next section.

Figure 24 shows Raman spectra of Ge_xS_{100-x}, ranging from 380 to 520 cm^{-1}. The peak at 470 cm^{-1} is assigned to the symmetric bond-stretching mode of S_8 ring molecules. It is well known that a peak (shoulder) appears at 461 cm^{-1} in liquid sulfur by the polymerization transition at 159 °C, where polymeric sulfur chains are thermally produced [91–93]. In $Ge_{10}S_{90}$, there is such shoulder. In $Ge_{20}S_{80}$, the relative intensity of the peak at 460 cm^{-1} to that at 470 cm^{-1} becomes larger. These features indicate that there are polymeric sulfur chains in $Ge_{10}S_{90}$ and $Ge_{20}S_{80}$. Indeed, there are S-S segments in the chainlike sequences in the models of $Ge_{10}S_{90}$ (Fig. 10) and $Ge_{20}S_{80}$ [Fig. 9(b)] and they could be related to the peak (shoulder) in the Raman spectra. In $Ge_{30}S_{70}$ and $Ge_{33}S_{67}$, a peak appears at 440 cm^{-1}. This peak is associated with the S-S bond of the edge dimer in "outrigger raft"[41,96]. Since the S-S bond is formed between two S atoms on two neighboring

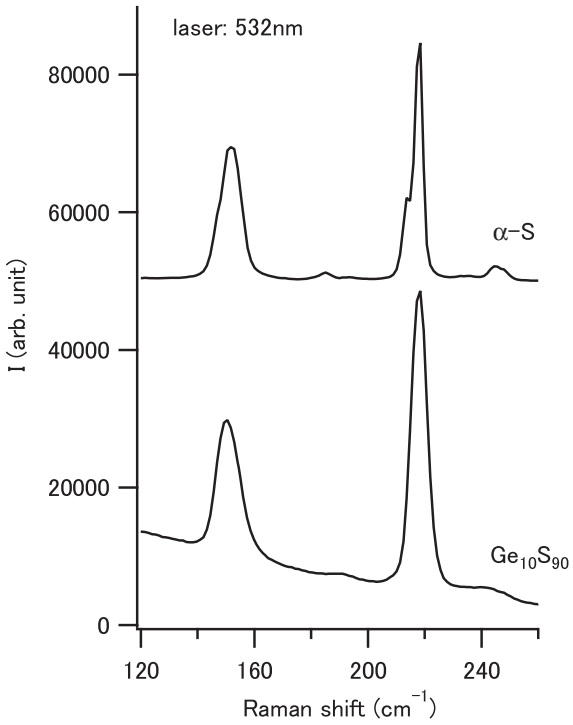

FIG. 23. Comparison of Raman spectra of α sulfur and $Ge_{10}S_{90}$ glasses, ranging from 120 to 250 cm^{-1}.

GeS_4 tetrahedra with only one Ge-S bond [98] [see Fig. 8(a)], there are more chances to have the S-S bond when two GeS_4 tetrahedra approach to each other, from the S_3-Ge-S-

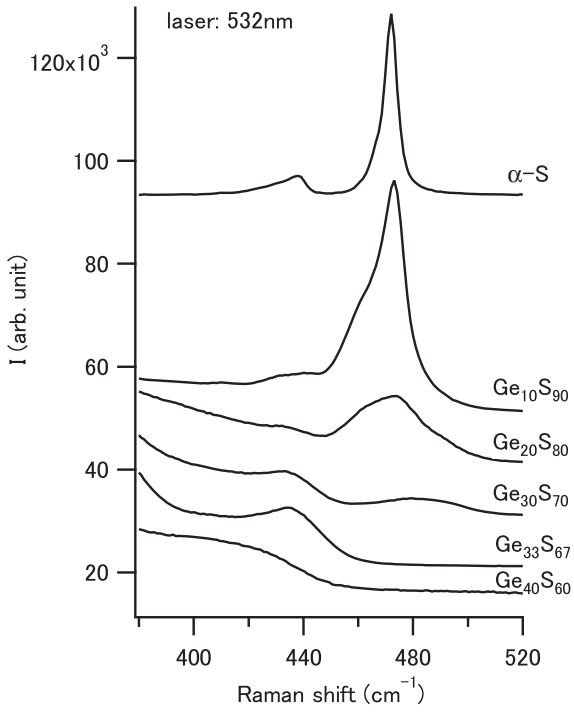

FIG. 24. Raman spectra of Ge_xS_{100-x}, ranging from 380 to 520 cm^{-1}.

S-Ge-S_3 sequence ($Ge_{20}S_{80}$) to the S_3-Ge-S-Ge-S_3 sequence ($Ge_{33}S_{67}$). The change of the peak intensity agrees with this expectation. Such a S-S bond can also be formed between two neighboring GeS_4 tetrahedra in $Ge_{40}S_{60}$ (Fig. 11).

The presence of a S_3-Ge-Ge-S_3 ethanelike unit, which includes a Ge-Ge homopolar bond, was often suggested based on the result of Raman spectroscopy [15,41,45,48]. According to Lucovsky *et al.* [15], the peaks at 240, 340, and 376 cm^{-1} are assigned to the vibrational modes of the ethanelike unit. Jackson *et al.* reproduced the spectrum from a first-principles molecular-dynamics study and they assigned the peaks at 254 and 366 cm^{-1} to the vibrational modes of the ethanelike units [45]. Those peaks are also observed in the Raman spectrum of $Ge_{33}S_{67}$ (GeS_2) in the present experiment (Figs. 21 and 22). In Sec. III A 1, we mentioned that the Ge-Ge bond in the S_3-Ge-Ge-S_3 ethanelike unit is not a major bond type in GeS_2 glasses. However, the result of the Raman spectra indicates that there are but small quantities of the Ge-Ge wrong bonds in GeS_2.

In the Raman spectra of $Ge_{40}S_{60}$, there are broad peaks at 220 and 250 cm^{-1}. Although the position of 250 cm^{-1} is the same as that of the vibrational mode of the S_3-Ge-Ge-S_3 ethanelike unit, Boolchand *et al.* suggested that the peak was assigned to the vibrational mode of the double layer in crystalline GeS, not the S_3-Ge-Ge-S_3 ethanelike unit. In the Raman spectra of a GeS crystal at room temperature, intensive peaks are observed at 50, 110, 210, and 240 cm^{-1} [39,99,100]. The lowest 50-cm^{-1} peak is related to the sliding of the double layers in the crystal. The peak at 110 cm^{-1} is assigned to the bond-bending mode while the peaks at 210 and 240 cm^{-1} are assigned to the bond-stretching modes. Among those peaks, the bond-stretching modes are supposed to "survive" even when the material changes from crystalline to amorphous phase. In fact, the S-Ge-S unit with a bridging Ge atom (Fig. 11) could be a fragment where bond-stretching occurs. Therefore, the peaks at 220 and 250 (240) cm^{-1} could be assigned to the bond-stretching modes of the S-Ge-S unit with a bridging Ge atom. The peak position can also be justified by a rough estimation of the vibrational frequency of a diatomic molecule using $\nu \sim (K/\mu)^{1/2}$, where μ and K are the reduced mass and the force constant, respectively [101]. Since the force constant must be proportional to the strength (length) of the bond, the vibrational frequencies of three types of bond would be ν(Ge-S: 2.44 Å) = 240 cm^{-1} < ν(Ge-S: 2.22 Å)= 340 cm^{-1} < ν(S-S: 2.04 Å)= 470 cm^{-1}. In our previous paper, we pointed out that there was a peak at 410 cm^{-1} in Ge-rich Ge-S glasses, and inferred that it was attributed to a single Ge-S chain, which was separated from the double layer [16]. The Ge-S bond in the chain is supposed to be the longer Ge-S bond, discussed in the previous section. However, the peak seems to indicate a different structure, and this should be solved by further structural studies.

2. *Spatial dependence in* $Ge_{10}S_{90}$ *glasses*

The Raman scattering spectra were taken by a micro-Raman spectrometer. In the measurement of $Ge_{10}S_{90}$, we observed inhomogeneous patterns on the image by the microscope as shown in Fig. 25. There are a homogeneous region and a grainlike region. Raman scattering measurement was performed for both of the regions as shown in Fig. 26. In the homogeneous region, there are both S_8 ring molecules and amorphous materials including GeS_4 tetrahedra because there are sharp peaks associated with S_8 ring molecules at 150, 220, and 470 cm^{-1} and a peak associated with corner-sharing GeS_4 tetrahedra at 340 cm^{-1}. Peaks in the low-frequency region below 100 cm^{-1} are broadened and overlapped to each other. This means that S_8 molecules in the homogeneous region do not form a perfect crystal, but form rather structure with amorphous character. We infer that S_8 ring molecules are embedded in tiny empty spaces in the Ge-S network. In the grainlike region, there are both S_8 ring molecules and amorphous materials including GeS_4 tetrahedra, too, because

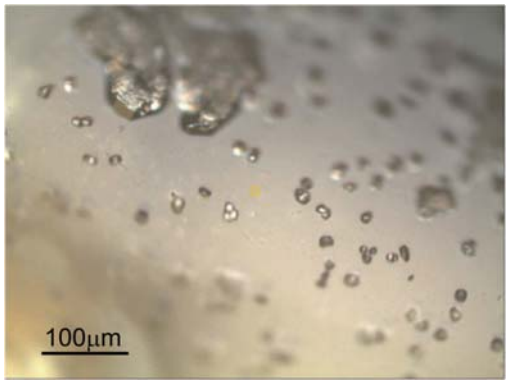

FIG. 25. Image of $Ge_{10}S_{90}$ glasses observed by a microscope.

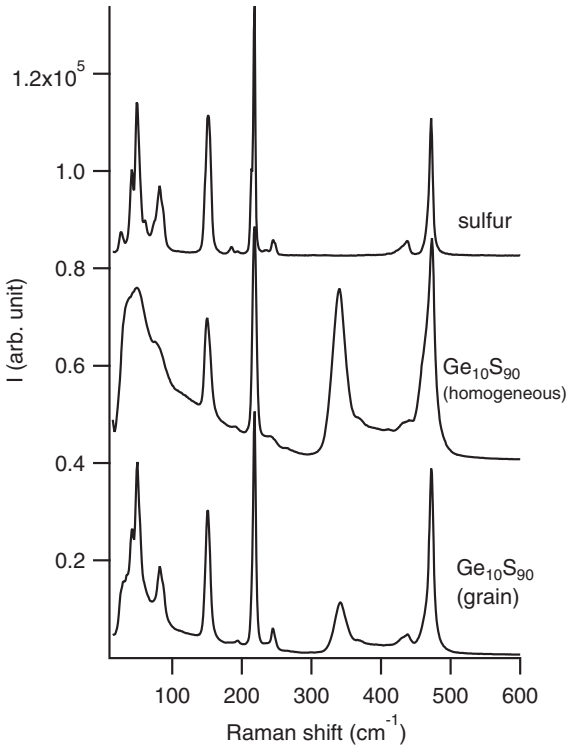

FIG. 26. Raman spectra of $Ge_{10}S_{90}$ glass in the homogeneous region and grainlike region together with the Raman spectrum of α sulfur.

there are sharp peaks associated with S_8 ring molecules at 150, 220, and 470 cm^{-1} and a peak associated with corner-sharing GeS_4 tetrahedra at 340 cm^{-1}. The peak intensity at 340 cm^{-1} is smaller than that in the homogeneous region. This means that the content of amorphous phase in the grainlike region is less than that in the homogeneous region. The peaks in the low-frequency region below 100 cm^{-1} are sharp as well as those of α sulfur. Therefore, there are crystals in the grainlike region. It is concluded that there are both crystalline and amorphous phases, but the crystalline phase is the majority in the grainlike region. The boundary between the crystalline and amorphous phases is not observed in the image with micrometer size, and is expected to be observed in nanoscopic scales. This coincides with a large small-angle x-ray scattering of $Ge_{10}S_{90}$ (Figs. 15 and 19) and a large small-angle neutron scattering of S-rich Ge-S glasses observed by Bychkov *et al.* [29]. We infer that crystallization can proceed even at room temperature because Bychkov *et al.* reported the time-dependent change of the small-angle neutron scattering [29], which would be caused by the change of crystalline phase/amorphous phase boundaries.

IV. CONCLUSIONS

We carried out the x-ray diffraction measurement of Ge_xS_{100-x} (10 x 40) glasses using high-energy x rays of synchrotron radiation and Raman scattering measurement. It was found from the measurements that the local, medium-range and nanoscopic orders change with increasing Ge content, and the network models of the glasses are proposed based on the results. In the stoichiometric composition of GeS_2 ($Ge_{33}S_{67}$), the network is composed of GeS_4 tetrahedral units, with corner-sharing (a dominant case) or edge-sharing connection. In the S-rich glasses, S atoms are inserted between the GeS_4 tetrahedra. This makes the network more flexible, and makes the voids (cages) smaller. In much S-richer glasses ($Ge_{10}S_{90}$), more S atoms are inserted between the GeS_4 tetrahedra. In the glasses, S_8 ring molecules are embedded in the network and can assemble to form crystals. This would be the biggest difference compared to the Ge-Se system. The glasses are regarded as *crystallized glasses* and their functionality will be of interest from the application's point of view. In the Ge-rich glasses, GeS_4 tetrahedra are three-dimensionally connected with bridging Ge atoms. The bridging Ge-S bond is weaker than the intratetrahedron bond and this makes the optical gap decrease, resulting in the changes in color and other optical properties. The decrease of the optical gap leads to a greater photosensitivity in the Ge-rich films [59,60] and it is interesting to explore new functionality in the Ge-rich glasses. The structural understanding obtained in this study will also provide considerable insight into the mechanism of the silver photodiffusion into amorphous Ge-S, which markedly depends on the Ge content. In conclusion, a structural transformation occurs in Ge_xS_{100-x} (10 x 40) network glasses with increasing Ge content. The nature of the connectivity fundamentally changes with increasing Ge content, and the structural changes manifest themselves in a wide spatial range from the atomic short-range to the nanoscopic large scale.

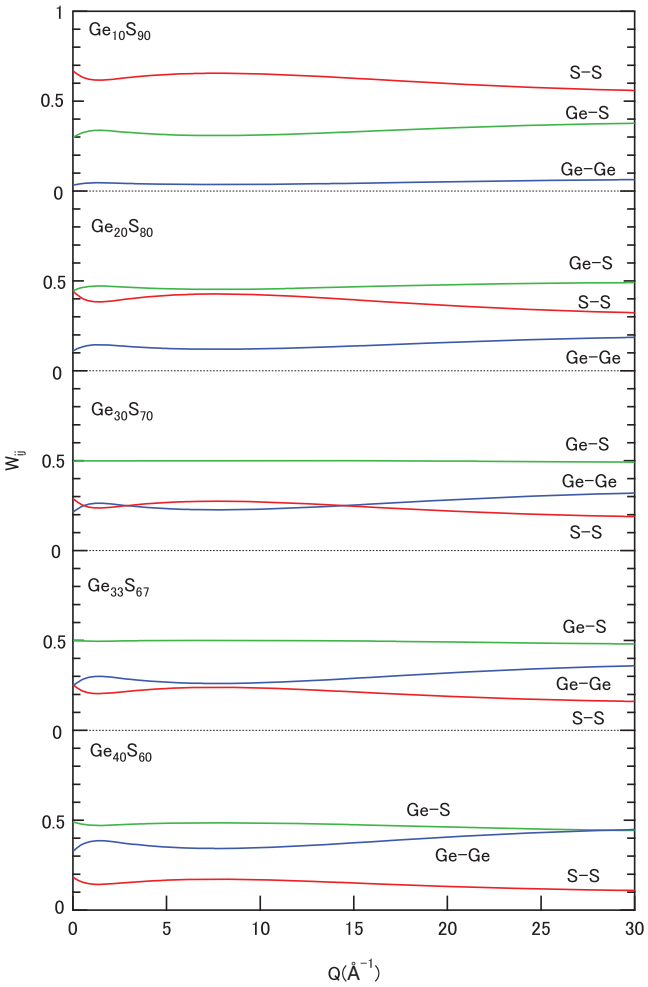

FIG. 27. Q dependence of the weighting factors W_{ij} for Ge_xS_{100-x} glasses.

ACKNOWLEDGMENTS

The x-ray diffraction measurements were performed on BL04B2 in SPring-8 under Project No. 2016B1414. The authors are grateful to Dr. Y. Onodera (Institute for Integrated Radiation and Nuclear Science, Kyoto University) and Dr. H. Arima (CROSS) for their invaluable discussion on the evaluation of coordination numbers from radial distribution functions. The authors would like to acknowledge the technical support of the Raman scattering measurement for T. Oyama and T. Soejima (JASCO). The authors would like to also acknowledge the technical support of the powder x-ray diffraction measurement in CROSS laboratory for Dr. T. Moyoshi. This research was supported by Award No. DE-NE0008691 sponsored by the Department of Energy's Nuclear Energy University Program (NEUP).

APPENDIX: THEORY OF THE COORDINATION NUMBER CALCULATION

Faber and Ziman [102] defined the partial structure factors $S_{ij}(Q)$ in their work on the electrical properties in liquid

binary alloys:

$$S_{ij}(Q) = 1 + \rho_0 \int [g_{ij}(r) - 1] \exp(-i\boldsymbol{Q} \cdot \boldsymbol{r}) d\boldsymbol{r}, \tag{A1}$$

where ρ_0 is the average number density of the sample, $g_{ij}(r)$ is the partial pair distribution functions. The Faber-Ziman total structural factor $S_{\mathrm{FZ}}(Q)$ is given by the equation [62,67]

$$\begin{aligned} S_{\mathrm{FZ}}(Q) &= \sum_{\alpha} \sum_{\beta} c_\alpha c_\beta \frac{f_\alpha(Q) f_\beta(Q)}{\langle f(Q) \rangle^2} S_{\alpha\beta}(Q) \\ &= \sum_{\alpha} \sum_{\beta} W_{\alpha\beta} S_{\alpha\beta}(Q), \end{aligned} \tag{A2}$$

where c_i $(i = \alpha, \beta) = N_i/N$ (N_i: the number of atoms i, N: the total number of atoms), $f(Q)$ is the atomic scattering factor

$$\langle f(Q) \rangle = c_1 f_1(Q) + c_2 f_2(Q), \tag{A3}$$

and the weighting factors $W_{\alpha\beta}$,

$$W_{\alpha\beta} = c_\alpha c_\beta \frac{f_\alpha(Q) f_\beta(Q)}{\langle f(Q) \rangle^2}. \tag{A4}$$

In neutron diffraction, the atomic scattering factor $f(Q)$ is replaced to the scattering length b, which is constant regardless of Q. Thus, W_{ij} is constant in neutron diffraction. On the other hand, W_{ij} depends on Q in x-ray diffraction [61]. This affects the accuracy in the estimation of the coordination number. It is also noted that $S_{\alpha\beta}$ cannot be distinguished from $S_{\beta\alpha}$ in the present experiment. Therefore, we define $W_{\alpha\beta}$ for $\alpha = \beta$ in this study as

$$W_{\alpha\beta} = 2 c_\alpha c_\beta \frac{f_\alpha(Q) f_\beta(Q)}{\langle f(Q) \rangle^2} \quad (\alpha = \beta). \tag{A5}$$

Following the definitions, we obtained the Q dependence of W_{ij} for $\mathrm{Ge}_x\mathrm{S}_{100-x}$ binary alloy, and the result is shown in Fig. 27.

For $\mathrm{Ge}_x\mathrm{S}_{100-x}$ binary alloy, the Faber-Ziman total structural factors of $\mathrm{Ge}_x\mathrm{S}_{100-x}$ are written as

$$\begin{aligned} S_{\mathrm{Ge}_x\mathrm{S}_{100-x}}(Q) = {} & W_{\text{Ge-Ge}} S_{\text{Ge-Ge}}(Q) + W_{\text{Ge-S}} S_{\text{Ge-S}}(Q) \\ & + W_{\text{S-S}} S_{\text{S-S}}(Q). \end{aligned} \tag{A6}$$

In general, the radial distribution functions RDF(r) have a relationship with the structure factors $S(Q)$ as

$$\mathrm{RDF}(r) = 4\pi r^2 \rho_0 + \frac{2r}{\pi} \int_{Q_{\min}}^{Q_{\max}} Q[S(Q) - 1] \sin(Qr) dQ. \tag{A7}$$

Using (A5) and (A6), $\mathrm{RDF}_{\mathrm{Ge}_x\mathrm{S}_{100-x}}(r)$ is written as

$$\begin{aligned} \mathrm{RDF}_{\mathrm{Ge}_x\mathrm{S}_{100-x}}(r) = {} & W_{\text{Ge-Ge}} \mathrm{RDF}_{\text{Ge-Ge}}(r) + W_{\text{Ge-S}} \mathrm{RDF}_{\text{Ge-S}}(r) \\ & + W_{\text{S-S}} \mathrm{RDF}_{\text{S-S}}(r). \end{aligned} \tag{A8}$$

Assuming that the peak in the experimentally obtained radial distribution functions is assigned to the i-j correlation, the area of the peak A is written as

$$A = W_{ij} \int_{r_{\min}}^{r_{\max}} \mathrm{RDF}_{i-j}(r) dr. \tag{A9}$$

Therefore, the coordination number N_{i-j} of j atoms around an i atom is

$$N_{i-j} = \frac{A}{W_{ij}} \times c_j. \tag{A10}$$

[1] *Photo-Induced Metastability in Amorphous Semiconductors*, edited by A. V. Kolobov (Wiley-VCH, Weinheim, 2003).

[2] A. V. Kolobov and J. Tominaga, *Chalcogenides-Metastability and Phase Change Phenomena* (Springer, Berlin, 2012).

[3] K. Tanaka and K. Shimakawa, *Amorphous Chalcogenide Semiconductors and Related Materials* (Springer, Berlin, 2014).

[4] Y. Kawamoto and S. Tsuchihashi, J. Am. Ceram. Soc. **52**, 626 (1969).

[5] R. Azoulay, H. Thibierge, and A. Brenac, J. Non-Cryst. Solids **18**, 33 (1975).

[6] J. C. Phillips, J. Non-Cryst. Solids **34**, 153 (1979).

[7] M. F. Thorpe, J. Non-Cryst. Solids **57**, 355 (1983).

[8] M. F. Thorpe, D. J. Jacobs, M. V. Chubynsky, and J. C. Phillips, J. Non-Cryst. Solids **266**, 859 (2000).

[9] P. Boolchand, D. G. Georgiev, and B. Goodman, J. Opt. Adv. Mater. **3**, 703 (2001).

[10] P. Boolchand, X. Feng, and W. J. Bresser, J. Non-Cryst. Solids. **293**, 348 (2001).

[11] M. V. Chubynsky and M. F. Thorpe, Curr. Opin. Solid State Mater. Sci. **5**, 525 (2001).

[12] A. Sartbaeva, S. A. Wells, A. Huerta, and M. F. Thorpe, Phys. Rev. B **75**, 224204 (2007).

[13] G. Lucovsky, F. L. Galeener, R. C. Keezer, R. H. Geils, and H. A. Six, Phys. Rev. B **10**, 5134 (1974).

[14] S. Sugai, Phys. Rev. B **35**, 1345 (1987).

[15] G. Lucovsky, R. J. Nemanich, and F. L. Galeener, in *Proceedings of the 7th International Conference on Amorphous and Liquid Semiconductors, Edinburgh, Scotland 1977*, edited by W. E. Spear (G. G. Stevenson, Dundee, Scotland, 1977), p.125.

[16] Y. Sakaguchi, D. A. Tenne, and M. Mitkova, J. Non-Cryst. Solids **355**, 1792 (2009).

[17] M. T. Kostyshin, E. V. Mikhailovskaya, and P. F. Romanenko, Fiz. Tverdogo Tela **8**, 571 (1966) [Sov. Phys. Solid State **8**, 451 (1966)].

[18] H. N. A. Yoshikawa, O. Ochi, and Y. Mizushima, Appl. Phys. Lett. **29**, 677 (1976).

[19] R. E. B. J. Hajto, P. J. S. Ewen, and A. E. Owen, Thin Solid Films **200**, 229 (1991).

[20] M. Mitkova and M. N. Kozicki, J. Non-Cryst. Solids **299**, 1023 (2002).

[21] M. Mitkova and M. N. Kozicki, in *Resistive Switching: From Fundamentals of Nanoionic Redox Processes to Memristive Device Applications*, edited by D. Ielmini and R. Waser (Wiley, Hoboken, NJ, 2015), Chap. 17.

[22] A. V. Kolobov and S. R. Elliott, Adv. Phys. **40**, 625 (1991).

[23] Y. Sakaguchi, H. Asaoka, Y. Uozumi, Y. Kawakita, T. Ito, M. Kubota, D. Yamazaki, K. Soyama, M. Ailavajhala, M. R. Latif, and M. Mitkova, Can. J. Phys. **92**, 654 (2014).

[24] Y. Sakaguchi, H. Asaoka, Y. Uozumi, Y. Kawakita, T. Ito, M. Kubota, D. Yamazaki, K. Soyama, M. Ailavajhala, M. R. Latif, K. Wolf, M. Mitkova, and M. W. A. Skoda, J. Phys.: Conf. Ser. **619**, 012046 (2015).

[25] Y. Sakaguchi, H. Asaoka, Y. Uozumi, Y. Kawakita, T. Ito, M. Kubota, D. Yamazaki, K. Soyama, M. Ailavajhala, K. Wolf, M. Mitkova, and M. W. A. Skoda, JPS Conf. Proc. **8**, 031023 (2015).

[26] Y. Sakaguchi, H. Asaoka, Y. Uozumi, Y. Kawakita, T. Ito, M. Kubota, D. Yamazaki, K. Soyama, G. Sheoran, and M. Mitkova, Phys. Status Solidi A **213**, 1894 (2016).

[27] Y. Sakaguchi, H. Asaoka, Y. Uozumi, K. Kondo, D. Yamazaki, K. Soyama, M. Ailavajhala, and M. Mitkova, J. Appl. Phys. **120**, 055103 (2016).

[28] N. Fueki, T. Usuki, S. Tamaki, H. Okazaki, and Y. Waseda, J. Phys. Soc. Jpn. **61**, 2814 (1992).

[29] E. Bychkov, M. Miloshova, D. L. Price, C. J. Benmore, and A. Lorriaux, J. Non-Cryst. Solids **352**, 63 (2006).

[30] A. Bytchkov, G. J. Cuello, S. Kohara, C. J. Benmore, D. Price, and E. Bychkov, Phys. Chem. Chem. Phys. **15**, 8487 (2013).

[31] S. Kohara, K. Suzuya, Y. Kashihara, N. Matsumoto, N. Umezaki, and I. Sakai, Nucl. Instrum. Methods, Phys. Res. Sect. A **467**, 1030 (2001).

[32] M. Isshiki, Y. Ohishi, S. Goto, K. Takeshita, and T. Ishikawa, Nucl. Instrum. Methods, Phys. Res. Sect. A **467**, 663 (2001).

[33] S. Kohara, M. Itou, K. Suzuya, Y. Inamura, Y. Sakurai, Y. Ohishi, and M. Takata, J. Phys.: Condens. Matter **19**, 506101 (2007).

[34] S. J. Rettig and J. Trotter, Acta. Crystallogr. C **43**, 2260 (1987).

[35] V. G. Dittmar and H. Schäfer, Acta. Crystallogr. **B31**, 2060 (1975).

[36] W. H. Zachariasen, Phys. Rev. **40**, 917 (1932).

[37] H. Wiedemeier and H. G. von Schnering, Z. Kristallogr. **148**, 295 (1978).

[38] A. Okazaki, J. Phys. Soc. Jpn. **13**, 1151 (1958).

[39] H. C. Hsueh, M. C. Warren, H. Vass, G. J. Ackland, S. J. Clark, and J. Crain, Phys. Rev. B **53**, 14806 (1996).

[40] S. Blaineau, P. Jund, and D. A. Drabold, Phys. Rev. B **67**, 094204 (2003).

[41] P. Boolchand, J. Grothaus, M. Tenhover, M. A. Hazle, and R. K. Grasselli, Phys. Rev. B. **33**, 5421 (1986).

[42] P. S. Salmon and I. Petri, J. Phys.: Condens. Matter **15**, S1509 (2003).

[43] I. Petri, P. S. Salmon, and H. E. Fischer, Phys. Rev. Lett. **84**, 2413 (2000).

[44] M. Cobb, D. A. Drabold, and R. L. Cappelletti, Phys. Rev. B **54**, 12162 (1996).

[45] K. Jackson, A. Briley, S. Grossman, D. V. Porezag, and M. R. Pederson, Phys. Rev. B. **60**, R14985 (1999).

[46] A. Ibanez, E. Philippot, S. Benazeth, and H. Dexpert, J. Non-Cryst. Solids **127**, 25 (1991).

[47] P. Armand, A. Ibanez, H. Dexpert, and E. Philippot, J. Non-Cryst. Solids **139**, 137 (1992).

[48] S. Blaineau and P. Jund, Phys. Rev. B **69**, 064201 (2004).

[49] R. J. Temkin, W. Paul, and G. A. N. Connell, Adv. Phys. **22**, 581 (1973).

[50] G. Etherington, A. C. Wright, J. T. Wenzel, J. C. Dore, J. H. Clarke, and R. N. Sinclair, J. Non-Cryst. Solids **48**, 265 (1982).

[51] J. Drahokoupil, O. Smotlacha, F. Fendrych, H. Klokočníková, and M. A. Kozlov, J. Non-Cryst. Solids **88**, 43 (1986).

[52] J. Akola, B. Beuneu, R. O. Jones, P. Jóvári, J. Kolář, I. Voleská, and T. Wágner, J. Phys.: Condens. Matter **27**, 485304 (2015).

[53] J. Robertson, Adv. Phys. **32**, 361 (1983).

[54] K. Hachiya, J. Non-Cryst. Solids **312-314**, 566 (2002).

[55] K. Hachiya, J. Non-Cryst. Solids **321**, 217 (2003).

[56] K. H. M. Seki and K. Yoshida, J. Non-Cryst. Solids **324**, 127 (2003).

[57] R. K. Pan, H. Z. Tao, H. C. Zang, C. G. Lin, T. Zhang, and X. J. Zhao, J. Non-Cryst. Solids **357**, 2358 (2011).

[58] Y. Kawamoto and S. Tsuchihashi, J. Am. Ceram. Soc. **54**, 131 (1971).

[59] Y. Sakaguchi, D. Tenne, and M. Mitkova, Phys. Status Solidi B **246**, 1813 (2009).

[60] M. Mitkova, A. Kovalskiy, H. Jain, and Y. Sakaguchi, J. Opt. Adv. Mater. **11**, 1899 (2009).

[61] B. E. Warren, *X-ray Diffraction* (Dover, New York, 1990).

[62] Y. Waseda, *The Structure of Non-Crystalline Materials* (McGraw-Hill, New York, 1980).

[63] H. Takebe, H. Maeda, and K. Morinaga, J. Non-Cryst. Solids **291**, 14 (2001).

[64] P. Armand, A. Ibanez, and E. Philippot, J. Solid State Chem. **104**, 308 (1993).

[65] A. Bouzid, S. L. Roux, G. Ori, M. Boero, and C. Massobrio, J. Chem. Phys. **143**, 034504 (2015).

[66] N. F. Mott and E. A. Davis, *Electronic Processes in Non-Crystalline Materials*, 2nd ed. (Oxford University Press, Oxford, 1979).

[67] S. R. Elliott, *Physics of Amorphous Materials*, 2nd ed. (Longman Scientific and Technical, Essex, 1990).

[68] K. Arai and H. Namikawa, Solid State Commun. **13**, 1167 (1973).

[69] I. Watanabe and T. Shimizu, Solid State Commun. **25**, 705 (1978).

[70] I. Watanabe, Y. Inagaki, and T. Shimizu, Japan. J. Appl. Phys. **15**, 1993 (1976).

[71] I. Watanabe, M. Ishikawa, and T. Shimizu, J. Phys. Soc. Jpn. **45**, 1603 (1978).

[72] V. Černý and M. Frumar, J. Non-Cryst. Solids **33**, 23 (1979).

[73] E. A. Zhilinskaya, V. N. Lazukin, N. K. Valeev, and A. K. Oblasov, J. Non-Cryst. Solids **124**, 48 (1990).

[74] Y. Kawamoto and S. Tsuchihashi, J. Am. Ceram. Soc. **54**, 526 (1971).

[75] J. Malek and J. Shanelova, J. Non-Cryst. Solids **243**, 116 (1999).

[76] C. Lin, L. E. Busse, S. R. Nagel, and J. Faber, Phys. Rev. B **29**, 5060 (1984).

[77] I. Petri and P. S. Salmon, J. Non-Cryst. Solids **293**, 169 (2001).

[78] S. R. Elliott, Nature (London) **354**, 445 (1991).

[79] J. C. Phillips, J. Non-Cryst. Solids **43**, 37 (1981).

[80] S. R. Elliott, Phys. Rev. Lett. **67**, 711 (1991).

[81] S. R. Elliott, J. Non-Cryst. Solids **182**, 40 (1995).

[82] S. R. Elliott, J. Phys.: Condens. Matter **4**, 7661 (1992).

[83] A. C. Wright, J. Non-Cryst. Solids **179**, 84 (1994).

[84] Q. Mei, C. J. Benmore, S. Sen, R. Sharma, and J. L. Yarger, Phys. Rev. B **78**, 144204 (2008).
[85] C. Crupi, G. Carini, M. Gonzalez, and G. D'Angelo, Phys. Rev. B **92**, 134206 (2015).
[86] B. Meyer, Chem. Rev. **76**, 367 (1976).
[87] A. C. Wright, S. W. Martin, D. L. Price, and F. L. Galeener, J. Non-Cryst. Solids **129**, 213 (1991).
[88] I. P. Kotsalas and C. Raptis, Phys. Rev. B **64**, 125210 (2001).
[89] M. Yamaguchi, T. Shibata, and K. Tanaka, J. Non-Cryst. Solids **232-234**, 715 (1998).
[90] M. Becucci, R. Bini, E. Castellucci, B. Eckert, and H. J. Jodl, J. Phys. Chem. B **101**, 2132 (1997).
[91] A. T. Ward, J. Phys. Chem. **72**, 4133 (1968).
[92] A. G. Kalampounias, K. S. Andrikopoulos, and S. N. Yannopoulos, J. Chem. Phys. **118**, 8460 (2003).
[93] K. S. Andrikopoulos, A. G. Kalampounias, O. Falagara, and S. N. Yannopoulos, J. Chem. Phys. **139**, 124501 (2013).
[94] G. Lucovsky, J. P. deNeufville, and F. L. Galeener, Phys. Rev. B **9**, 1591 (1974).
[95] G. Lucovsky, R. L. Nemanich, S. A. Solin, and R. C. Keezer, Solid State Comm. **17**, 1567 (1975).
[96] K. Murase, T. Fukunaga, Y. Tanaka, K. Yakushiji, and I. Yunoki, Phys. B (Amsterdam) **117**, 962 (1983).
[97] R. Steudel and H. Mausle, Z. Anorg. Allg. Chem. **478**, 156 (1981).
[98] P. M. Bridenbaugh, G. P. Espinosa, J. E. Griffiths, J. C. Phillips, and J. P. Remeika, Phys. Rev. B. **20**, 4140 (1979).
[99] J. D. Wiley, W. J. Buckel, and R. L. Schmidt, Phys. Rev. B **13**, 2489 (1976).
[100] H. R. Chandrasekhar, R. G. Humphreys, and M. Cardona, Phys. Rev. B **16**, 2981 (1977).
[101] J. R. Ferraro, K. Nakamoto, and C. W. Brown, *Introductory Raman Spectroscopy*, 2nd ed. (Academic, London, 2003).
[102] T. E. Faber and J. M. Ziman, Philos. Mag. **11**, 153 (1965).